

Technical Report #: TR-2024-4828042

---

# Final Report: Validation of Underwater Radiated Noise Modelling via Specific Ship Measurement

April 2024

**American Bureau of Shipping**  
275 Slater Street, Suite 1003  
Ottawa, Ontario, K1P 5H9

© 2024 American Bureau of Shipping  
All rights reserved.





---

## OUR MISSION

The mission of ABS is to serve the public interest as well as the needs of our members and clients by promoting the security of life and property and preserving the natural environment.

---

## Executive Summary

This report summarizes the technical work performed to develop, test, and validate various predictive models for ship-induced underwater radiated noise. For this objective, a dedicated sea trial for the Canadian Coast Guard vessel *CCGS Terry Fox*, a twin-screw icebreaker, was conducted. Detailed sea trial plan and instrumentation were designed and executed in accordance with the *ABS Guide for Classification Notation Underwater Noise and External Airborne Noise* (January 2024).

A wide variety of models and tools for predicting underwater radiated noise predictive tools were adopted to re-produce the source noise levels for comparison with the sea trial results. The models ranged from empirical formulas based on broad databases to high-fidelity computational fluid dynamics and computational hydroacoustics models. These models possess different levels of fidelity, demand for efforts to set up, and demand for computational resources to implement. From the comparison of the predicted radiated noise level spectra with that measured from the sea trial, it was found that the quick, empirical formulas are very useful in providing an envelope for the potential noise levels for a vessel in the early design state. The medium level modeling, involving numerical simulation using the Boundary Element Method and semi-empirical cavitation models, required a reasonable level of effort and showed improvements when compared with the sea trial results. The high-fidelity method, employing fully numerical simulation from first principles, did not show further improvements. With such high resource demand, the high-fidelity simulations could only attain a frequency of 300 Hz for the present study. Therefore, the application of the fully computational fluid and acoustic simulation to ship-induced noise prediction needs further improvement.

With the findings from the present study, especially the strengths and weaknesses of each methodology, a future plan for model improvement can be made based on the lessons learned through this study.



This page intentionally left blank

## Table of Contents

<b>1</b>	<b>INTRODUCTION .....</b>	<b>7</b>
<b>2</b>	<b>SEA TRIALS AND INSTRUMENTATION .....</b>	<b>8</b>
2.1	In-Water Data Collection Trials – Vessel Details .....	8
2.2	In-Water Data Collection Trials – Test Location and Conditions .....	9
2.3	Data Collection Trials – System .....	10
2.3.1	In-Water Measurements .....	10
2.3.2	Onboard Airborne Noise Measurements .....	14
2.3.3	Structure-Borne Noise Measurements.....	14
2.4	In-Water Data Collection Trials – Data Collection .....	15
2.5	Data Analysis for Quality Assurance .....	21
<b>3</b>	<b>PREDICTION OF SHIP-INDUCTED URN .....</b>	<b>23</b>
<b>4</b>	<b>EMPIRICAL MODELS FOR URN ASSESSMENT (LOW-FIDELITY METHODS) .....</b>	<b>24</b>
4.1	ABS Ship Propeller Noise Prediction Program .....	24
4.2	Propeller Noise Spectrum Program (ProSpec) .....	26
4.3	URN assessment for <i>CCGS Terry Fox</i> using empirical formulas .....	26
<b>5</b>	<b>MEDIUM-FIDELITY URN ASSESSMENT .....</b>	<b>29</b>
5.1	ETV method .....	29
5.2	Dynamic Bubbles App .....	29
5.3	URN assessment for the <i>CCGS Terry Fox</i> using Medium-Fidelity Methods .....	30
5.3.1	CFD-simulated wake field as input to PROCAL .....	30
5.3.2	Noise Assessment Using ETV Method For Tip Vortex Cavitation .....	35
5.3.3	Noise Assessment Using Dba Method For Sheet Cavitation .....	36
5.3.4	Combined Noise Levels For The Subject Vessel .....	38
<b>6</b>	<b>HIGH-FIDELITY URN ASSESSMENT .....</b>	<b>40</b>
6.1	Methodologies .....	40
6.2	CFD Methodology For The Propeller-Induced Cavitating Flow Field .....	41
6.3	CFD simulation results .....	42
6.4	Acoustic Model Setup .....	46
6.4.1	Acoustic computational domain .....	46
6.4.2	Boundary conditions for acoustic analysis .....	47
6.4.3	Placement of the numerical hydrophones .....	49
6.4.4	Results of iCFD Analysis .....	50
6.5	Results of acoustic analysis .....	51
6.6	Machinery-induced URN .....	54
6.6.1	Stage one .....	55
6.6.2	Stage two .....	57
6.6.3	Stage three .....	57
6.6.4	Analysis results .....	57
<b>7</b>	<b>Discussion .....</b>	<b>64</b>



- 8 COMMERCIAL SYSTEM DESIGN AND DEVELOPMENT ..... 67**
  - 8.1 Work Completed..... 67**
  - 8.2 Overall Design Approach ..... 67**
  - 8.3 Path to Completion and Commercialization..... 71**
    - 8.3.1 Review and finalize schematic and PCB layout for initial fabrication..... 71
    - 8.3.2 Build and test prototype hardware and verify device drivers. .... 72
    - 8.3.3 Write data handling code for Coral data logging/storage in removeable media.. 72
    - 8.3.4 Write Ethernet data transfer software for transmission to computer..... 72
    - 8.3.5 Build and integrate full system and calibrate accelerometer response..... 72
    - 8.3.6 Prepare signal processing and display software for crew-facing system..... 72
    - 8.3.7 Write API for integration with third party systems..... 73
    - 8.3.8 Deploy test system onboard a vessel of opportunity selected for best value proposition including opportunity for validation and follow-on marketing..... 73
- 9 CONCLUSIONS ..... 74**
- References..... 76**

## 1 INTRODUCTION

American Bureau of Shipping (ABS) actively supports the maritime industry's rising demand for quieter ships. In addition to developing the classification requirements, which are provided through the *ABS Guide for Classification Notations Underwater Noise and External Airborne Noise* [1], significant efforts are being devoted to developing the current state of the art for underwater radiated noise, which include: (1) developing predictive methods and tools and (2) evaluating mitigation measures that can be applied in the ship design and operation.

The maritime industry has been carrying out active research and tool development in recent years to predict the broadband noise emitted from a cavitating propeller and the tonal noise at the frequencies associated with propeller rotation. A vast amount of field measurement data was collected to evaluate the patterns of noise emission from different types of vessels and the impact on the environment. The main gap, however, is that the available measurement data sets mostly do not associate the vessel information required as part of the input for the validation of the methods for predicting underwater radiated noise (URN). For commercial vessels, the main source of URN is the propeller, especially when cavitating. Machinery equipment such as the main engine can also be an important contributor, especially at low vessel speeds. A less prominent, yet still relevant, source is the water flow around the ship. Depending on the level of complexity, the URN prediction typically involves detailed modeling of the ship hull form, propeller(s), interaction between the hull and the propeller(s), and machinery configuration. Simplified methods used for quick evaluation of different design options at the early design stage may be less demanding but still need the vessel information, which is often missing in the existing measurement data sets.

The objective of this project was to further verify and validate the URN predictive tools through dedicated sea trial measurements of the noise radiating from a specific vessel. This study brought together the in-situ measurement and the validation of URN predictive methods and tools through a coherent measurement-validation scheme. To this end, ABS first identified the subject vessel, the Canadian Coast Guard vessel *CCGS Terry Fox*, which was believed to be suitable for producing vessel-induced noise data for the present study. This vessel is an icebreaker. It has twin screws, a common propulsive configuration for ferries, offshore support vessels, and other ships which often operate near the habitats of marine mammals that are sensitive to ship-borne noise. With the collected noise data from the sea trials, different tiers of modeling methodologies and tools were developed and verified in predicting the URN of the vessel for the same conditions. The strengths and weaknesses of each method were noted through a comparison of the predicted URN versus the actual, measured data.

## 2 SEA TRIALS AND INSTRUMENTATION

The dedicated sea trial was conducted for the *CCGS Terry Fox* (IMO 8127799; Ice Class: Arctic Class 4), including onboard and underwater radiated noise measurements. The sea trial procedure and data processing were in accordance with ABS requirements [1].

### 2.1 In-Water Data Collection Trials – Vessel Details

The trials collected shipboard data at the same time as capturing in-water data, per the requirements of the ABS guide [1].

On June 19, 2023, the Autonomous Ocean System Laboratory Team, in the Department of Ocean and Naval Architectural Engineering at Memorial University of Newfoundland, performed tests to assess the underwater radiated noise from the *CCGS Terry Fox* as shown in . The detailed instrumentation was designed and supported by eSonar. More detail about the instrumentation is provided in Section 8. Table 2.1 shows the main specifications of the *CCGS Terry Fox*. Table 2.2 shows the main specifications of its propulsion system.



**Figure 2-1 The CCGS Terry Fox during the project's sea trials (June 19, 20203)**



**Table 2.1 Main specifications of the CCGS Terry Fox**

Quantity		Value	Unit
Length OA	$L_{OA}$	88.0	[m]
Beam	$B$	17.8	[m]
Service draft	$d$	8.3	[m]
Gross Tonnage	$GT$	4,234	[GT]
Maximum speed	$V_{S,max}$	16.0	[kn]
Nominal propulsion power	$P_{eng,tot}$	17.3	[MW]
Arctic Class	$AC$	4	[-]

**Table 2.2 Main specifications of the CCGS Terry Fox's propulsion system components**

Quantity		Value	Unit
<i>Machinery</i>			
Engine nominal power, at 100% load	$P_{eng,max}$	4,265	[kW]
Number of cylinders	$N_{cyl}$	8	[-]
Engine nominal speed	$n_{eng}$	600	[rpm]
Gearbox reduction ratio	$\gamma$	4.625	[-]
<i>Controllable Pitch Propeller</i>			
Diameter	$D_{prop}$	4.800	[m]
Number of blades	$Z$	4	[-]
Nominal rotational speed	$n_{prop}$	129.73	[rpm]
Zero-thrust pitch angle at 70% $R$	$\Phi_{min}$	-0.86	[deg]
Maximum pitch angle at 70% $R$	$\Phi_{max}$	25.92	[deg]

The vessel is equipped with 4 Stork-Werkspoor medium-speed diesel engines (model 8TM410LR) and 2 Caterpillar generator sets (model 351B). Each generator set delivers 1030 kW at 1200 RPM (revolutions per minute).

## 2.2 In-Water Data Collection Trials – Test Location and Conditions

The URN measurement location was selected in consultation with the CCGS Terry Fox's Captain and Chief Engineer. The tests were performed in Conception Bay, Newfoundland (Figure 2-2 ). The location was selected because of the sheltered deep waters. During the tests, the wind speed was 13 km/h or lower and waves were 1 m in height or lower. The water depth at the test site was ~ 200 m.

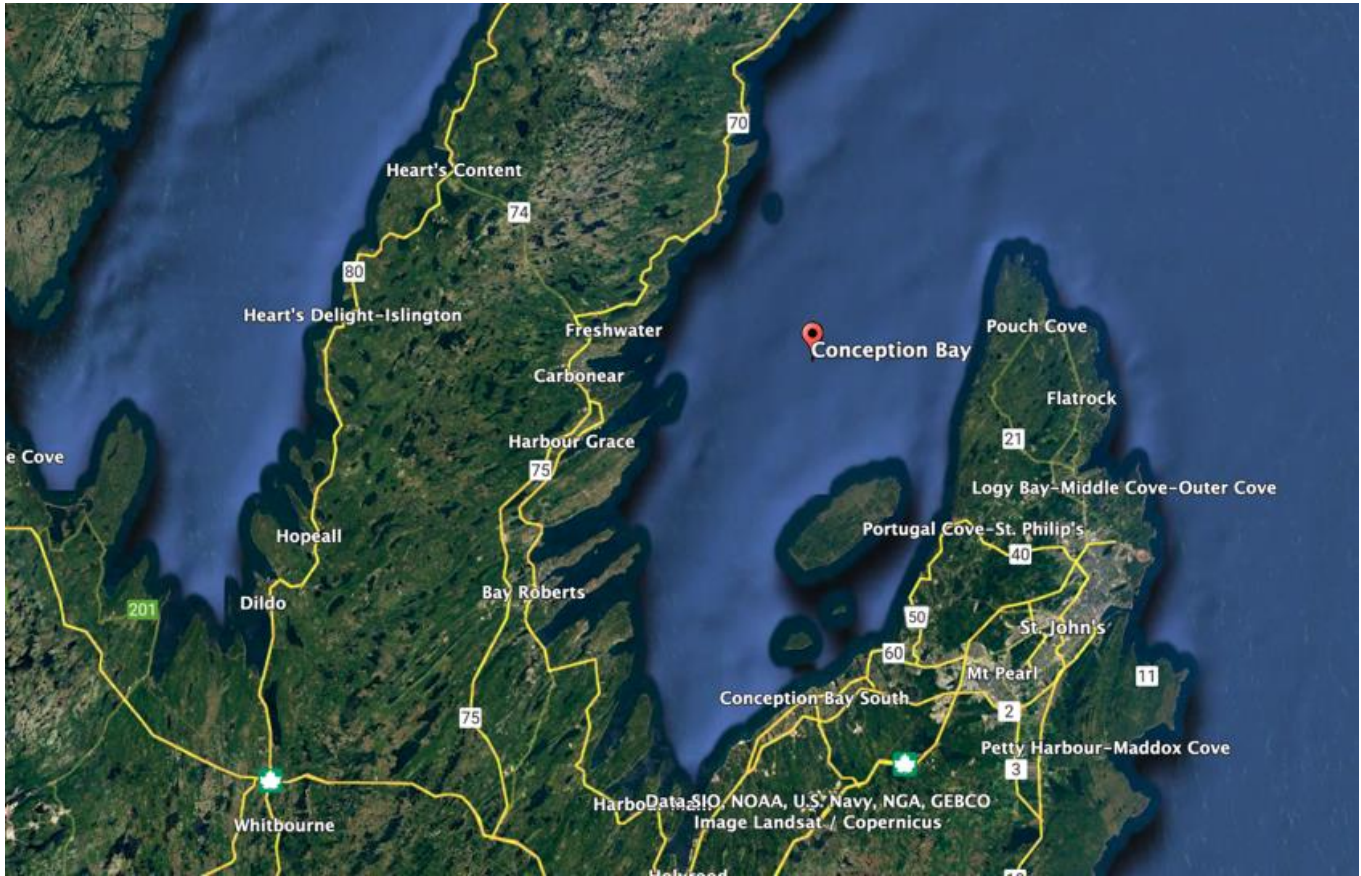


**Figure 2-2 Sea trial location, Conception Bay, Newfoundland**

### 2.3 Data Collection Trials – System

The project team implemented a fully integrated data collection plan that encompassed both onboard measurements of vibration at key locations including directly at the engine beds, and internally on hull plates proximate to the propellers to capture both cavitation and propulsion generated vibration. The plan was to measure propeller-induced hull structure-borne noise, and airborne and structure-borne noise from the prime movers. The data collected onboard the vessels was used to understand the contribution of each noise source to underwater radiated noise and would allow for a detailed characterization of the sources.

#### 2.3.1 In-Water Measurements

A floating system was selected to minimize the effect of current flow noise. The system consists of a GPS equipped buoy to which 3 tethered hydrophones, equally spaced along a 100 m cable which also provides power for the hydrophones. Further details about the instruments are as follows.

The hydrophones are Ocean Sonics 24-bit Smart Hydrophone-200 kHz (Model RB9-ETH), synchronized digital hydrophones that sample data at 32 kHz. (Figure 2-3 )

The buoy is an Ocean Sonics drifting buoy (Model BOS-W) with built-in GPS and Wi-Fi (Figure 2-4 )

The hydrophones are configured for daisy chaining together and for final connection to the communications buoy at the surface. The buoy has local Wi-Fi capability with sufficient strength for its signal to be picked up onboard the bridge of the vessel for real time data access and quality control.



**Figure 2-3 Digital Hydrophone: IcListen with Ethernet output**



**Figure 2-4 Surface Data Collection Buoy with Wi-Fi**

To increase the accuracy of the URN levels calculated, a Conductivity, Temperature, and Depth (CTD) measurement of the water column using a Seabird 25 CTD system equipped with a Sealogger Plus data recording system (Figure 2-5 ) was performed.



**Figure 2-5 Conductivity, Temperature, and Depth (CTD) sensor**

### 2.3.2 Onboard Airborne Noise Measurements

Onboard airborne noise measurements were performed in the engine room to characterize the prime movers and the generators as airborne noise sources. Airborne noise measurements were performed using:

- Larson Davis Sound level meter (Model 831C) with 51.2 kHz sample rate 30  $\mu$ s Peak rise time
- Larson Davis Omnidirectional Noise Source (Model BAS001) generating sound power up to 117 dB in a frequency range from 50 Hz to 12.5 kHz
- Larson Davis Class 1 SoundAdvisor Sound Level Meter (Model 831C)
- Larson Davis Precision Sound Level Calibrator (Model CAL200)

### 2.3.3 Structure-Borne Noise Measurements

The complete system for structure-borne noise contained:

- National Instrument Data Acquisition Cards models NI-9234 (four input) and NI-9230 (three input), collecting data at 24-bit and 51.2K samples/s;
- PCI accelerometers (Model 352C33) with a frequency range from 10 to 10 kHz
- Instrumented PCI hammer (Model LW38121)
  - PCB uniaxial accelerometers (Model 352C33)
  - National Instruments data acquisition systems NI-9234

Structure-borne noise was measured by PCB Piezoelectronics shear accelerometers installed at key locations as follows:

- In the ship double bottom in correspondence of the propeller to measure propeller-induced onboard structure-borne noise
- On the prime mover foundations to measure the diesel engines structure-borne noise - diesel engine foundation of Engine #4
- On the generator foundations to measure the generator structure borne noise - the gen-set foundation of gen-set #1

The sensors cover propeller-induced noise and machinery-induced vibration.

## 2.4 In-Water Data Collection Trials – Data Collection

Figure 2-6 shows the vessel paths of the sea trials at Conception Bay as well as the location of the drifting buoy used for tethering the hydrophones for measuring the URN during the tests.

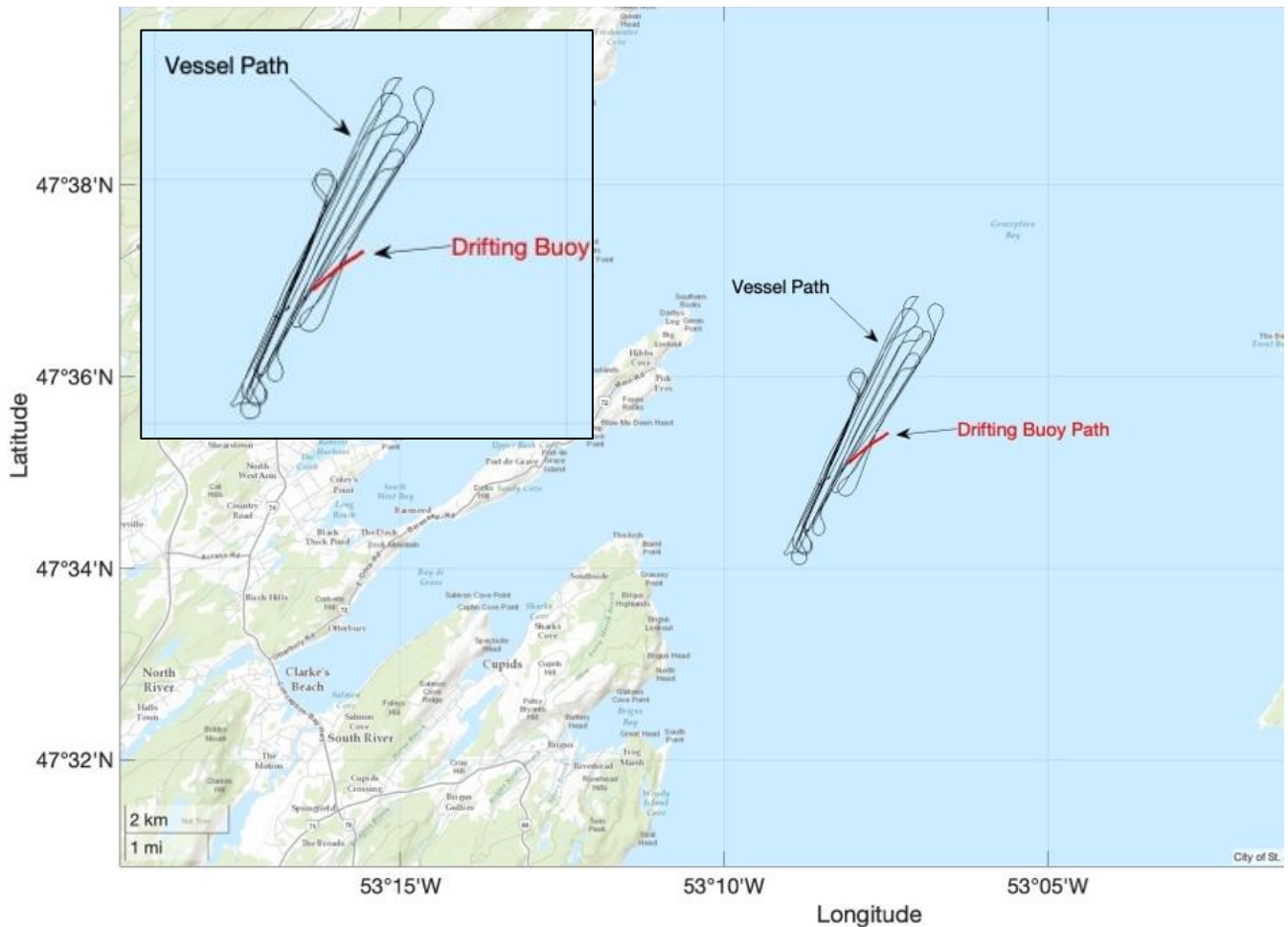


**Figure 2-6 Vessel paths and the drifting buoy location for the tests at Conception Bay, Newfoundland.**

Tests were performed on June 19, 2023, from 06:30 to 18:15. The vessel was tested at three different speeds: 6 knots, 8 knots, and 12 knots. In addition, the URN measurement was also performed at an advance speed of 0 knots, when the vessel was at the Closest Point of Approach (CPA). After the test, we measured the ocean background noise, by moving the vessel 6 km away from the drifting buoy.

Figure 2-7 shows the layout of the measuring instruments, in accordance with the ABS requirements [1]. The buoy was equipped with a GPS unit to locate its position at each instant of time and evaluate the CPA.

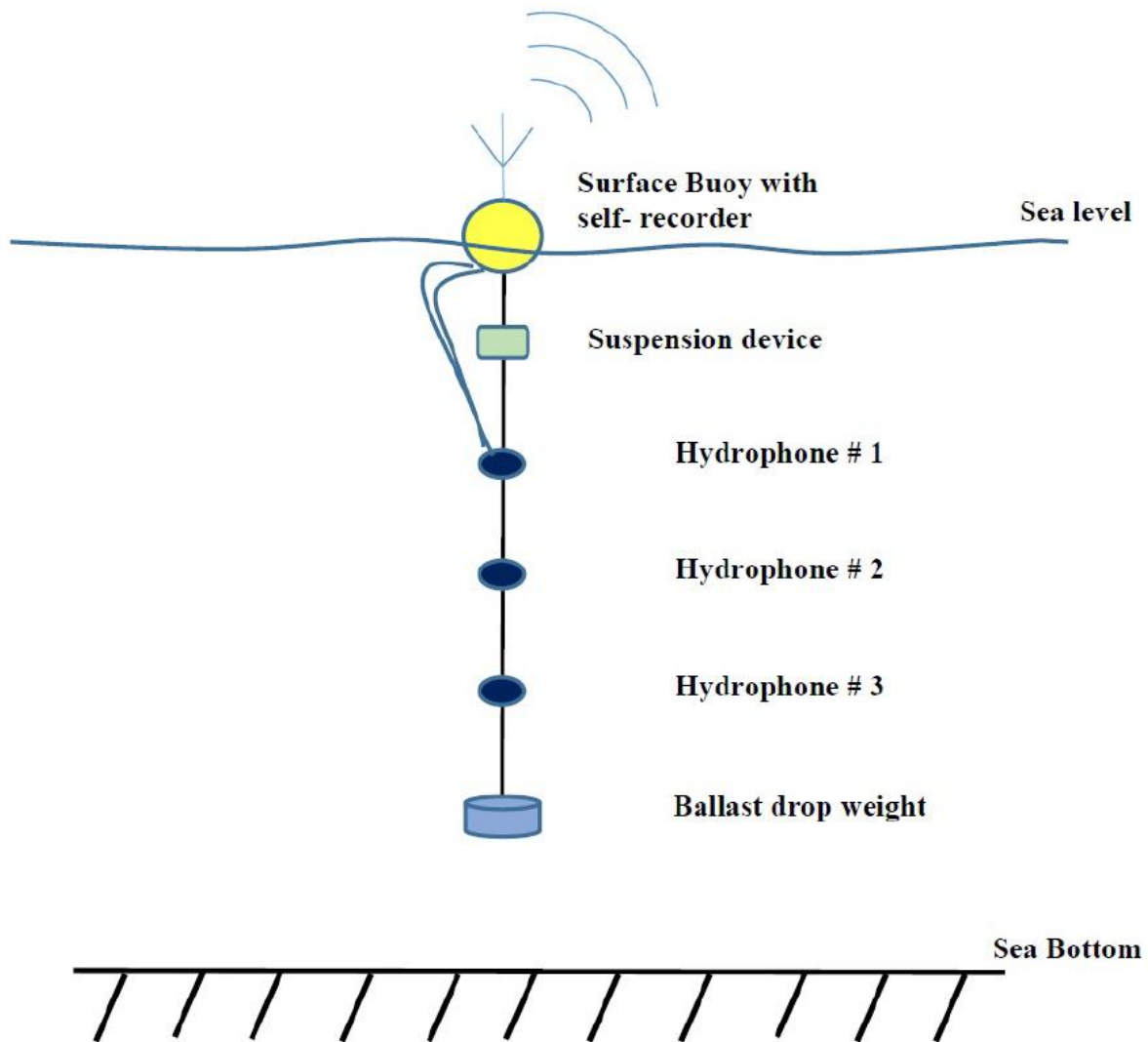


**Figure 2-7** The *in-situ* measuring system for the sea trials

At each advance speed, the vessel traveled along each path as shown in Figure 2-8 twice, to have two measurements of URN on the starboard side and two URN measurements on the port side.



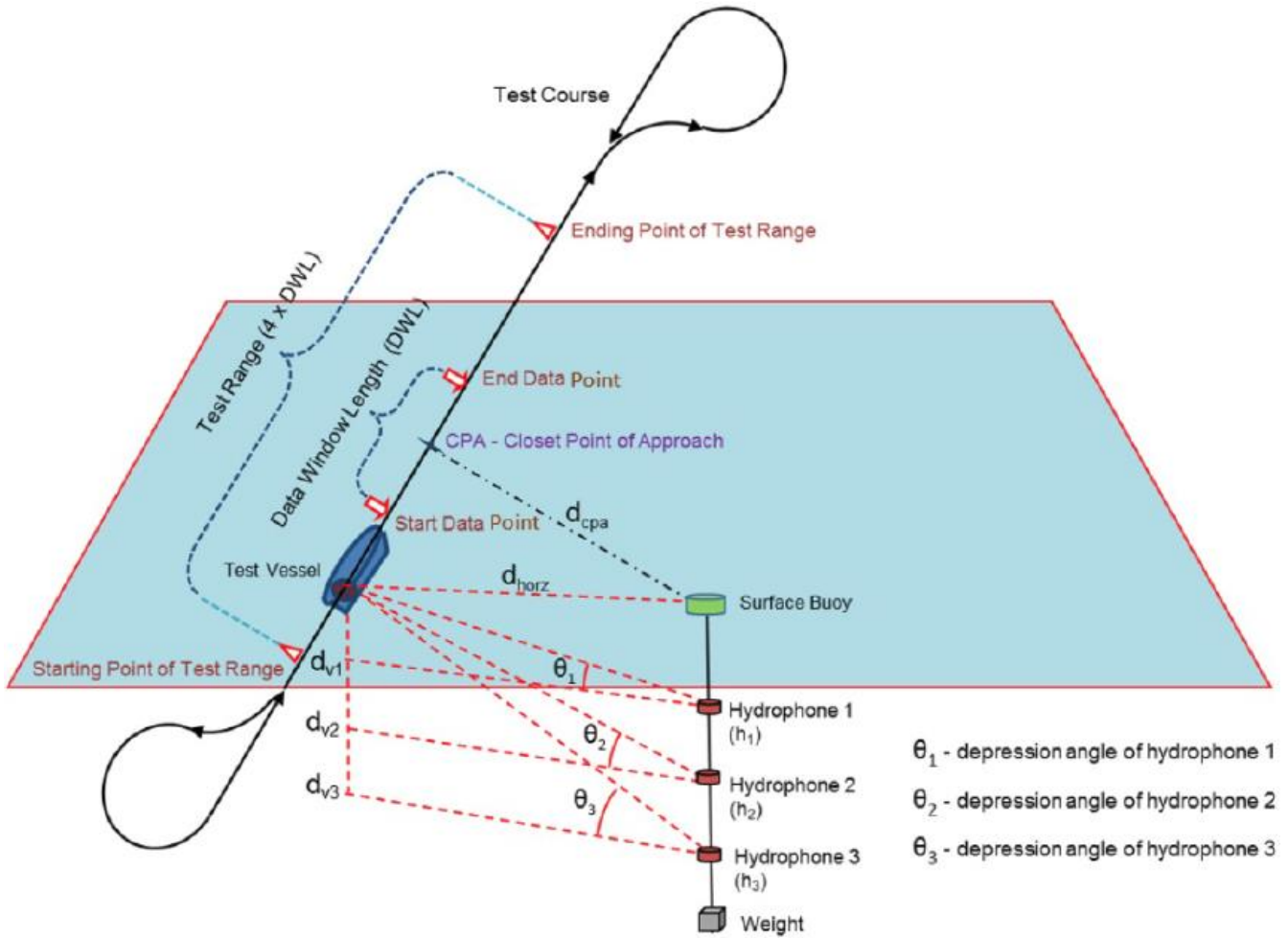


**Figure 2-8 Underwater noise measurement configuration - Beam Aspect Test Course**

A CTD measurement of the water column was made from the drifting buoy during the trials.

The project team measured structure-borne noise at the main diesel engine foundations, at the genset foundations, and in the double-bottom in way of the propellers. Figure 2-9 and Figure 2-10 show the installation of the accelerometers onboard in preparation for the trials.

Airborne noise measurements were made in the engine room and the gen-set room. Figure 2.11 shows the team members planning for the testing. The structure-borne noise data acquisition was performed in the vessel's steering room as shown in Figure 2.12. A buoy tender was used to deploy the hydrophone array (Figure 2.13).



**Figure 2-9 Accelerometer installed in the ship double bottom and at machinery base**

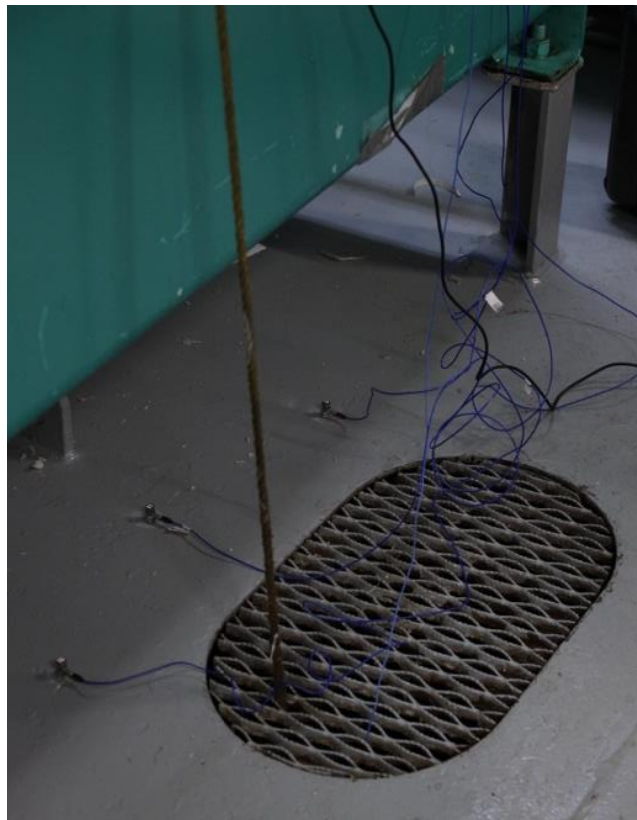


**Figure 2-10 Accelerometers installed to measure propeller-induced hull vibration**



**Figure 2-11 Sea trial test planning**



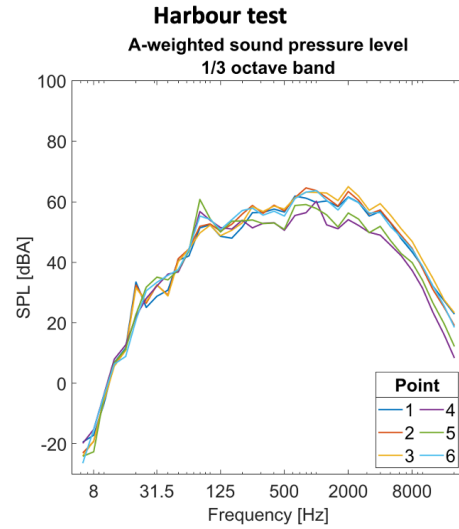
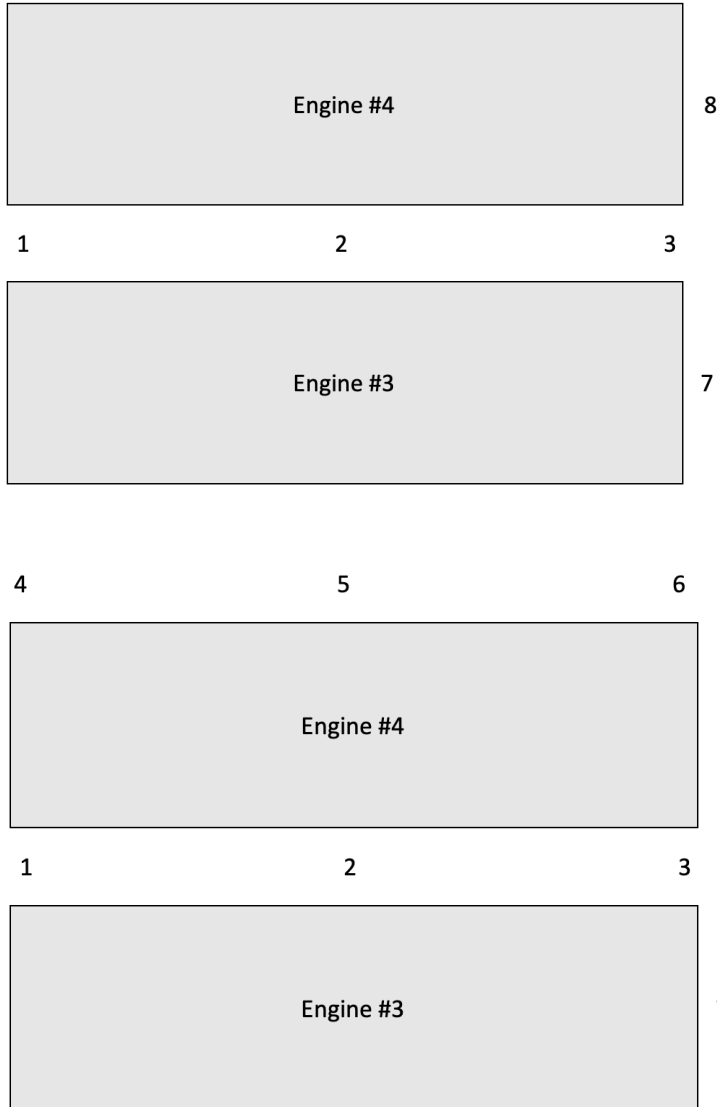
**Figure 2-12 Structure-borne noise data acquisition in the vessel's steering room**



**Figure 2-13 Hydrophone array deployment**

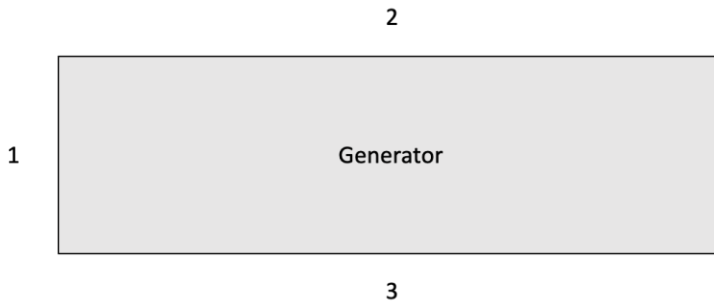
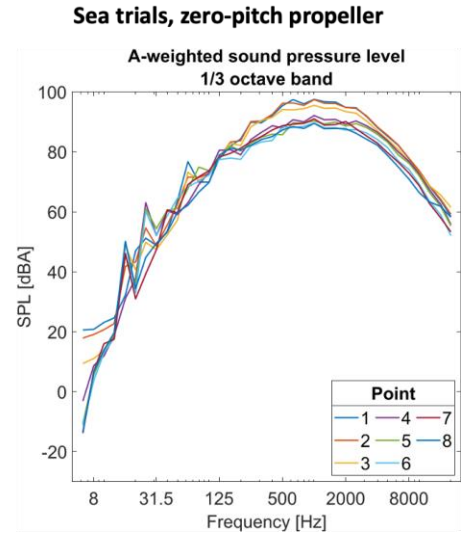
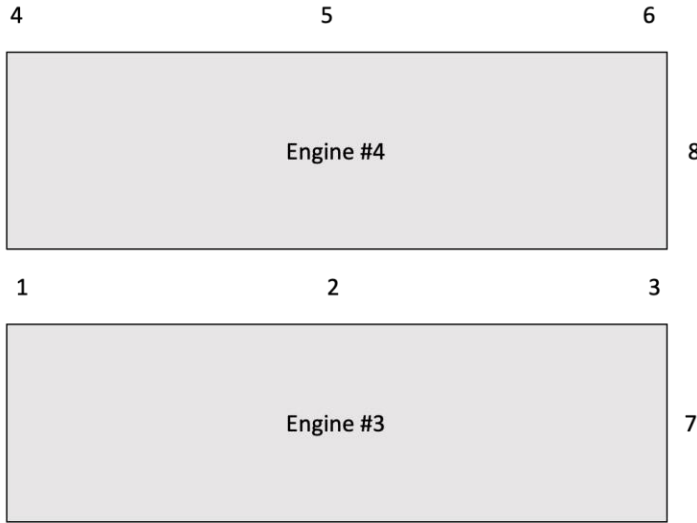
## 2.5 Data Analysis for Quality Assurance

Data collected during the trials was analyzed for quality assurance. Figure 2.14 shows some sample data collected during the trials.



Sea trials, zero-pitch propeller

Point	LAeq
1	108.1
2	107.9
3	106.8
4	102.1
5	101.1
6	100.9
7	99.8
8	99.1



**Harbour test**

Point	LAeq
1	98.2
2	105.5
3	104.4

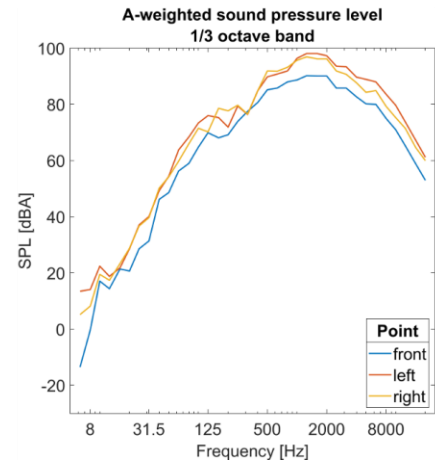


Figure 2-14 Sample data collected during the sea trial and examined for quality assurance

### 3 PREDICTION OF SHIP-INDUCED URN

The methodologies that ABS has adopted for predicting ship-induced URN in ambient water has multiple tiers, each of which has a different level of fidelity:

- Simple tools based on empirical formulas (low-fidelity)
- Numerical simulation based on Boundary Element Method (BEM) (medium-fidelity)
- Numerical simulation using Computational Fluid Dynamics and Computational Hydroacoustics (high-fidelity)

As expected, higher fidelity methods will demand more computational resources and more time to complete than the lower fidelity ones.

Different quantities are used to represent URN levels. The sound pressure level (SPL) is the sound power at a specific frequency or integrated over a specific frequency band (such as the 1/3 octave band) as received at a specific field point. The radiated noise level (RNL) represents the equivalent sound power at the acoustic source by adjusting for the transmission loss, which is assumed to be a spherical spreading loss:

$$RNL = SPL + 20 \log_{10} \left( \frac{r}{r_{ref}} \right) \quad (3.1)$$

where  $r$  denotes the distance between the acoustic source and the field point,  $r_{ref}$  denotes a standard reference distance which is often taken as 1 m. The second term on the right side of Eq. (3.1) represents the transmission loss,  $TL$ . For the present study, the “field point” is a hydrophone where the measured URN data is available. The acoustic source is defined as the center of the propeller on the same side to the vessel center plane as the hydrophones. The URN as received or predicted at each hydrophone can be converted into an  $RNL$ . The prediction of the noise source level should be based on the average of the  $RNL$ 's from all three hydrophones [1].

## **4 EMPIRICAL MODELS FOR URN ASSESSMENT (LOW-FIDELITY METHODS)**

In the early design stage when neither the hull form nor the detailed propeller information has been determined, simple methods can be used for estimating broadband noise levels. Several semi-empirical models have been developed by the shipping industry in the past decades and proven to be effective at predicting underwater radiated noise. Two software packages were used in the present project, namely: (1) ABS Ship Propeller Noise Prediction Program (ABS PropNoise) and (2) Propeller Noise Spectrum Program (ProSpec).

### **4.1 ABS Ship Propeller Noise Prediction Program**

ABS Ship Propeller Noise Prediction Program (“ABS PropNoise”) is an in-house research tool that uses semi-empirical formulas for predicting ship-induced URN including the influence of propeller cavitation.

ABS PropNoise includes four noise prediction models:

- Brown model
- Ross/Fraser model
- Wittekind model
- SNAME TR 3-37 model



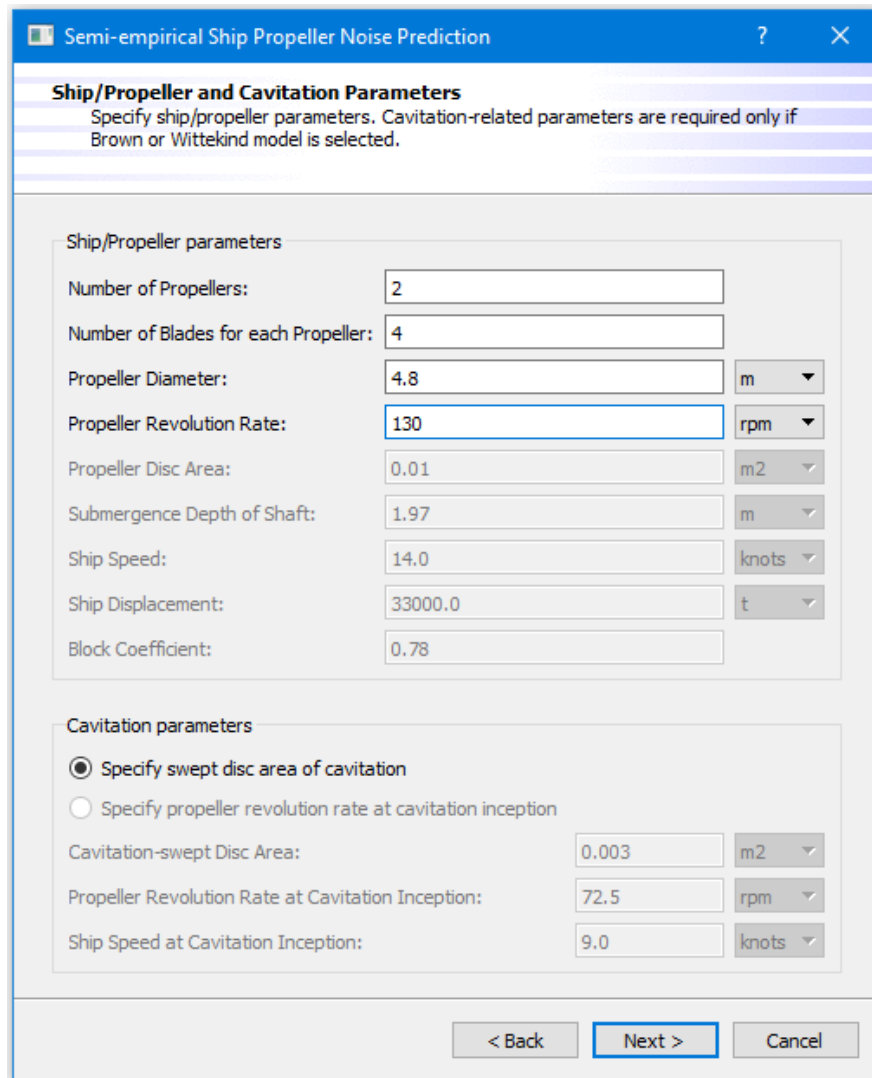


**Figure 4-1 User interface of ABS PropNoise for specifying propeller and cavitation parameters**

These empirical models were created based upon broad databases that have been widely applied as general guidance for the design purposes. The key input parameters for the empirical models usually include the number of propellers, the number of blades of each propeller, the propeller diameter, the propeller revolution rate, the propeller disc area, the shaft submergence depth, and other parameters including ship speed, displacement, block coefficient, as well as cavitation-related parameters such as the cavitation swept area and the propeller revolution rate at cavitation inception (as required for the Brown model) or the ship speed at cavitation inception (as required for the Wittekind model and the SNAME T&R 3-37 model). For example, for the Ross/Fraser model only four parameters are needed, which are the number of propellers, number of blades for each propeller, propeller diameter, and propeller RPM, as shown in **Figure 4-1**. Either the narrow band (with 1 Hz bandwidth) or the 1/3 octave band can be used for setting the frequency grid points. For more details about the formulation of the empirical models refer to Ref. [2].

## 4.2 Propeller Noise Spectrum Program (ProSpec)

The ProSpec software, developed by the Cooperative Research Ships (CRS) [3], relies on a semi-empirical model for prediction of URN levels induced by either non-cavitating or cavitating marine propellers. The model was originally developed by Angelopoulos et al. [4] at British Marine Technology (BMT) in the late 1980s based on the existing full-scale noise range data (presented in the 1/3 octave band) obtained from vessel sea trials. It also adopted a novel approach to model the cavitating or non-cavitating component of the spectrum. The model was also tuned with the data for single-screw fishery research vessels equipped with fixed pitch propellers.

The ProSpec software consists of three modules:

- A module for non-cavitating noise based on aeronautical formulations for propeller noise
- A module for cavitation inception to predict the cavitation inception number
- A module for cavitation to predict the peak frequency and the magnitude of the noise level spectrum

The method firstly predicts a cavitation inception point at which the cavitation noise starts to contribute to the overall spectrum levels. The noise levels below the cavitation inception point are assumed to be generic as obtained from aeronautical studies, where various methods and dominant parameters for helicopter rotor noise have been adopted. The overall spectrum levels are assumed to be composed of non-cavitating and cavitating noise components. This assumption determines the contribution (due to cavitation) to the noise spectrum levels of a surface vessel by logarithmically subtracting the non-cavitating component from the noise range measurements. The calculated components are defined with universal functions, and the frequency point is also defined within the developed model and by utilizing a trend line, where each of the components is expected to experience a maximum sound pressure level.

## 4.3 URN assessment for *CCGS Terry Fox* using empirical formulas

For the present study, the fundamental vessel specifications, propeller parameters and operating conditions of the *CCGS Terry Fox* are shown in Table 4.1. The analysis was performed for the sea trial condition with a vessel speed of 12 knots and a propeller rotational speed of 130 RPM.

**Table 4.1 Input data for predicting URN of the Terry Fox using empirical formulas**

Ship length (m)	88.0
Ship breadth (m)	17.8
Draft (m)	8.3
Ship displacement (MT)	4,234
Ship cruising speed (knot)	12
Block coefficient	0.577
Freeboard (m)	0.8
Number of propellers	2
Propeller diameter (m)	4.8
Boss ratio	0.141
Number of blades for each propeller	4
Total expanded blade area ratio	0.544
Propeller RPM	130
Submergence depth of shaft (m)	5.5

The sound levels predicted by ABS PropNoise (4 models) and ProSpec, as well as the sea trial measurements, are plotted together in **Figure 4-2**. It can be observed that except for the lower frequency range (0 to 100 Hz) the sound levels from different sources are close to one another. The predicted noise levels seem to constitute an upper bound for the measured noise levels at frequencies under 100 Hz. The agreement between the predicted and measured noise levels is especially good for frequencies higher than 100 Hz. All empirical formulas predicted the power-law decay of the 1/3 octave sound power for frequencies above 1000 Hz. It should be noted that the predicted noise levels only include the contributions from the propellers, whereas the measured noise levels included all constituents such as propeller- and machinery-induced noises.

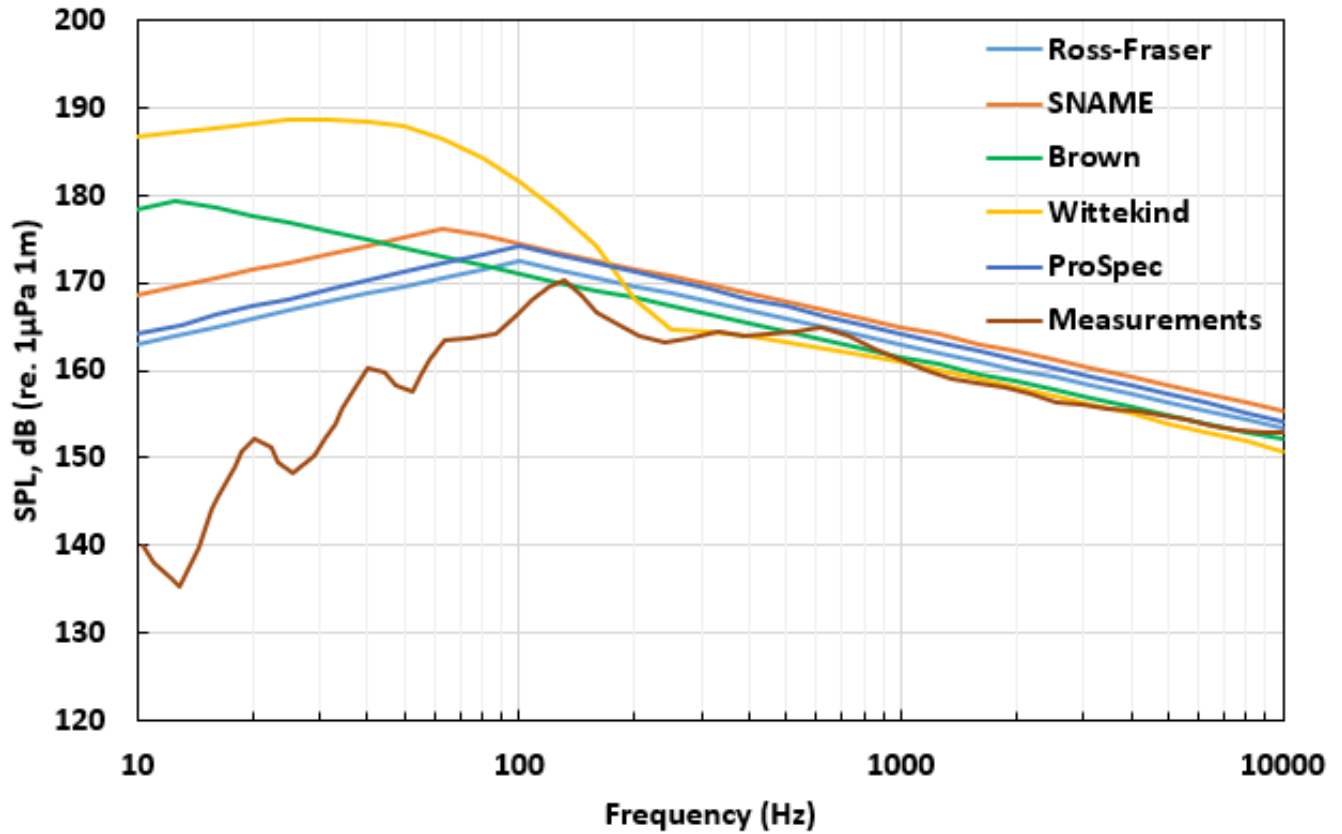


Figure 4-2 Propeller-induced noise spectrum levels based on five semi-empirical models (expressed in the 1/3 octave band)

## 5 MEDIUM-FIDELITY URN ASSESSMENT

At this fidelity level, ABS has adopted two analysis tools, both developed by CRS: (1) the ETV (Empirical cavitating Tip Vortex) method and (2) the dBA (Dynamic Bubbles APP) model. These tools rely on a BEM-based numerical code, PROCAL (a well verified and documented package by CRS), to provide the propeller-induced flow field. More specifically, the PROCAL code can be used to predict unsteady sheet cavitation on propeller blades operating in a ship wake, which could also result in hull-pressure fluctuations. Meanwhile, the graphical user interface PROVIDE (developed by DRDC Atlantic within the CRS) can be used to pre-process propeller geometries, generate surface panels, manage computations, and post-process results. PROCAL is still under development. As reported by CRS, some capabilities (such as Brown's model and the ETV model) will be integrated in the code. For more information about CRS PROCAL, one may refer to its User's Guide [5].

The key input to PROCAL is the effective wake field of the ship in which the propeller operates. Historically, this wake field could be obtained by a rescaling of a measured model-scale wake field. ABS has instead developed a coupling procedure for transferring a CFD-simulated wake flow field to PROCAL.

### 5.1 ETV method

The ETV model can predict the radiated noise due to the propeller tip vortex cavitation. The ETV model is based on an empirical model developed by Raestad [6] using the Tip Vortex Index (TVI) method. The model development is also based on onboard measurements of radiated noise from a large number of cruise vessels. To implement the ETV model, the tip vortex strength is obtained from PROCAL computations using the circulation strength at  $0.95R$  ( $R$  being the propeller radius) as a reference value. For the radiated noise in the far-field, the results are presented as the equivalent acoustic source strength at 1 m distance from the source.

The ETV method is still under development by CRS. The latest version of the ETV model is the ETV-3 model, which was used in the present study. The ETV model can be executed in the Microsoft Excel environment with the ease of data pre- and post-processing. The input data from PROCAL can be entered into the Excel spreadsheet to generate the radiated noise spectra. For more detail about the ETV tool, one may refer to Refs. [7], [8], and [9].

### 5.2 Dynamic Bubbles App

The Dynamic Bubbles App (abbreviated as "dBA") is a CRS software tool for predicting and analyzing broadband cavitation noises due to the sheet cavitation off the propeller blades. It is based on the theory of bubble dynamics and relies on PROCAL to provide flow field information around the propeller blades.

To analyze the URN produced by the oscillating bubbles resulting from cavitation, two models are integrated in dBA: (1) A single bubble model and (2) Matusiak's model, which helps predict the URN

generated by the partial shedding of sheet cavities on the propeller blades. For more details about the software package, one may refer to Ref. [10].

### 5.3 URN assessment for the *CCGS Terry Fox* using Medium-Fidelity Methods

#### 5.3.1 CFD-simulated wake field as input to PROCAL

PROCAL requires input of the vessel effective wake field in which the propeller operates. Alternatively, ABS first obtained a nominal wake field from a CFD simulation without the propeller. The nominal wake field was then transformed into the effective wake field using a utility tool “PIF\_WAKE” that often accompanies PROCAL.

The CFD simulation of the bare hull was performed at full scale using OpenFOAM (version 1812). The CFD model solved the fully three-dimensional Reynolds-Averaged Navier-Stokes (RANS) equations using the Finite Volume Method (FVM). The  $k-\omega$  SST turbulence model was used with wall functions to resolve the turbulent boundary layers over the hull and other appendage surfaces. The Volume-of-Fluid (VOF) method in OpenFOAM was improved with a modified compression term to stabilize the simulation and track the free surface movement. For the coordinate system, the right-hand rule applies. The origin of the coordinate system is the intersection of the Fore Perpendicular and the waterline with the  $X$ -axis directed from the bow to the stern, the  $Y$ -axis toward starboard, and the  $Z$ -axis pointing vertically upwards.

For the medium-fidelity level of prediction of URN, a high-quality hull geometry was first prepared (**Figure 5-1**). Hexpress (version 10.1, Cadence) was used for computational mesh generation. **Figure 5-2** shows the generated volume mesh around the hull. Local mesh refinements were applied near the free surface, the stern, and around the hull to resolve the ship-generated wave pattern and the wake field of the hull. The free-surface refinement zones were smoothly stretched towards the outlet boundary to damp out the hull-induced waves. The cell count of the entire computational mesh was approximately 3.7 million.

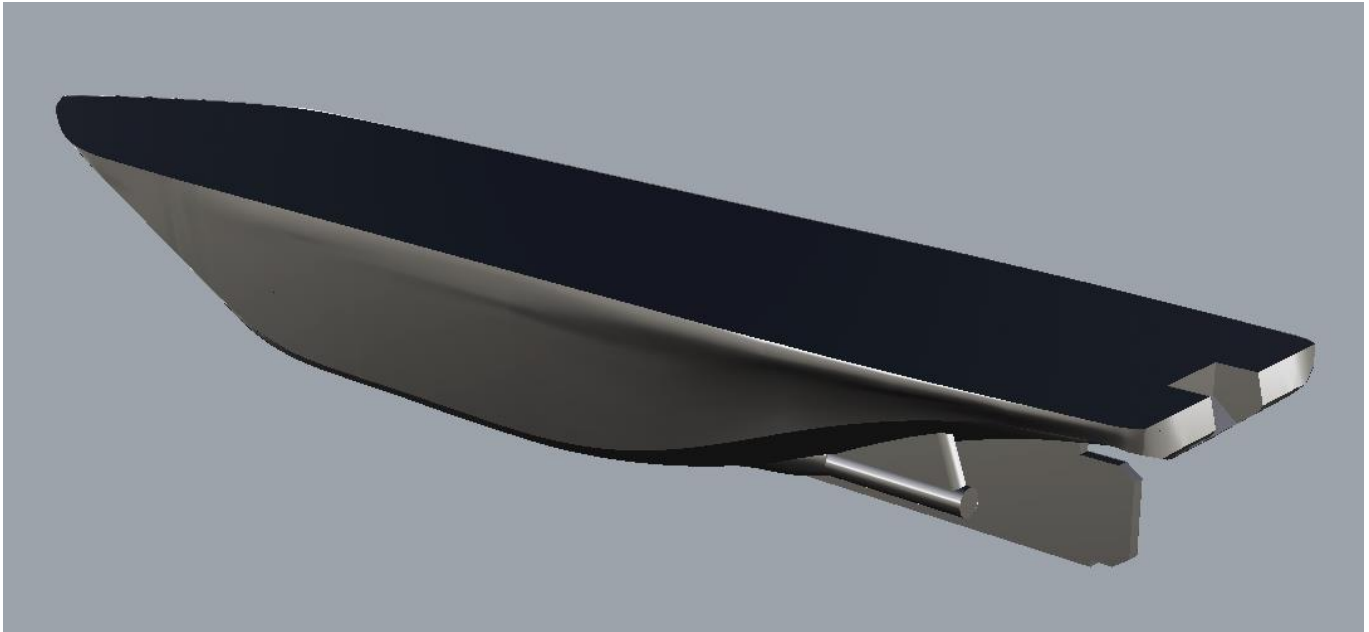


**Figure 5-1** Geometry of the subject vessel, the *CCGS Terry Fox*

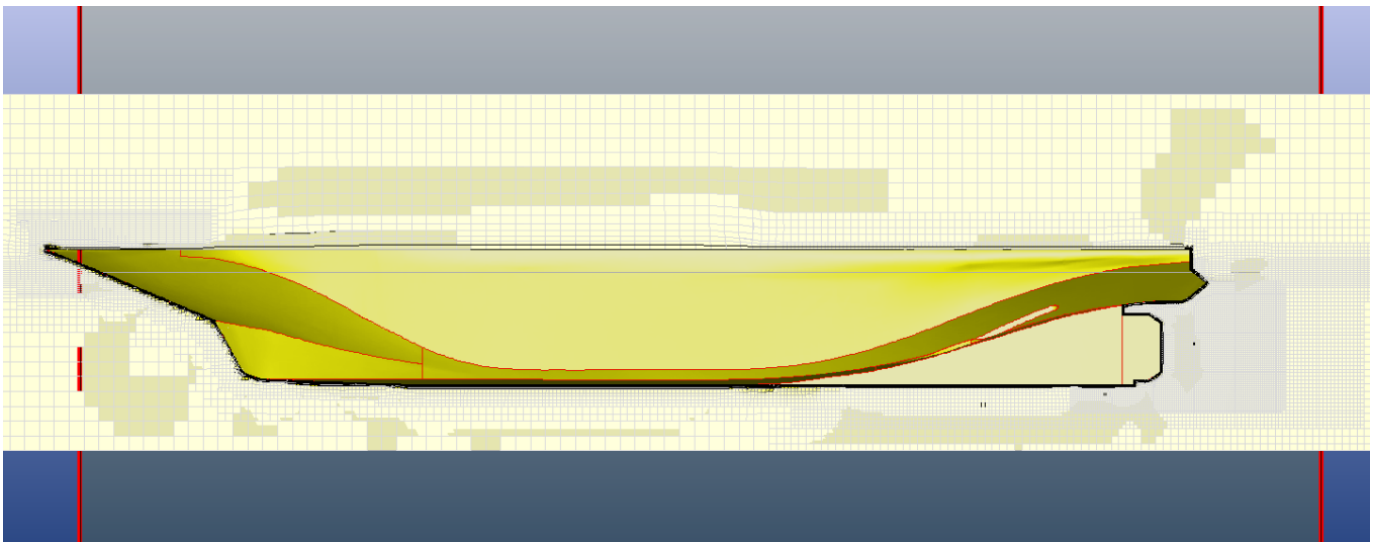


**Figure 5-2** Volume mesh of the *CCGS Terry Fox* along the center-plane

**Figure 5-3** shows the Kelvin wave pattern after the vessel reached a steady state, in terms of the vessel resistance, at a speed of 12 knots. Figure 3.6 shows the simulated nominal wake field as viewed along the propeller plane. Since the actual propellers were not considered in the simulation, the wake field is different from the effective wake field. This discrepancy was resolved by means of the CRS utility tool, PIF\_WAKE, and the effective wake field is shown in **Figure 5-4** for the port-side propeller.

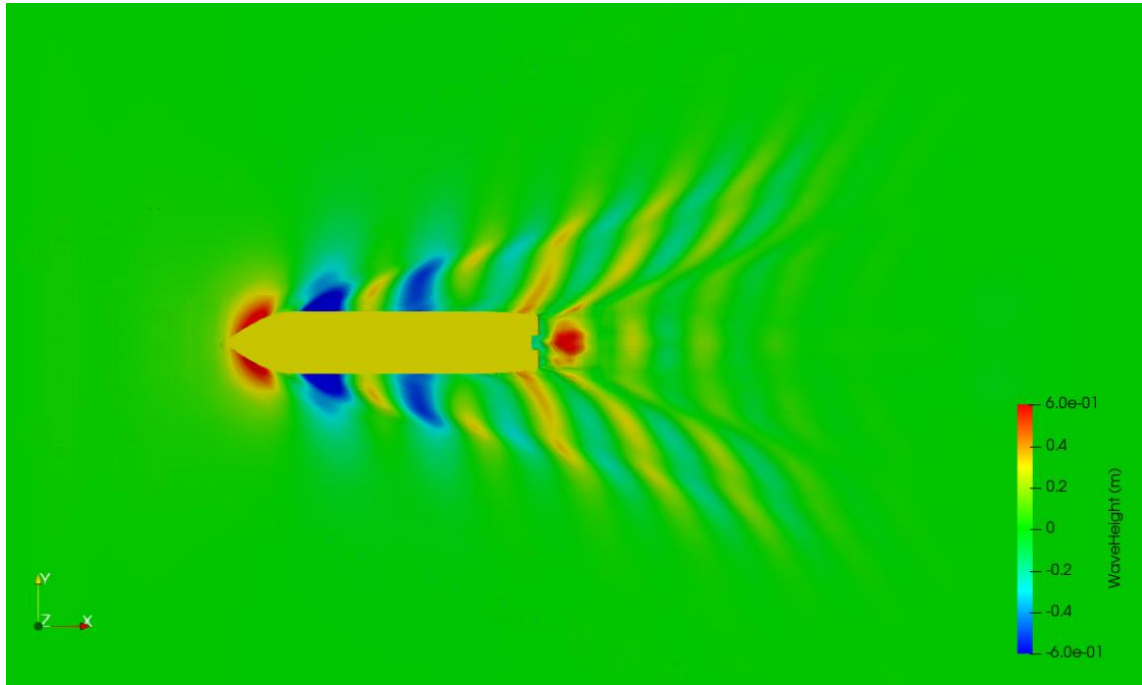


Figure 5-3 CFD-simulated Kelvin wave pattern of the bare hull of the *CCGS Terry Fox* at a speed of 12 knots

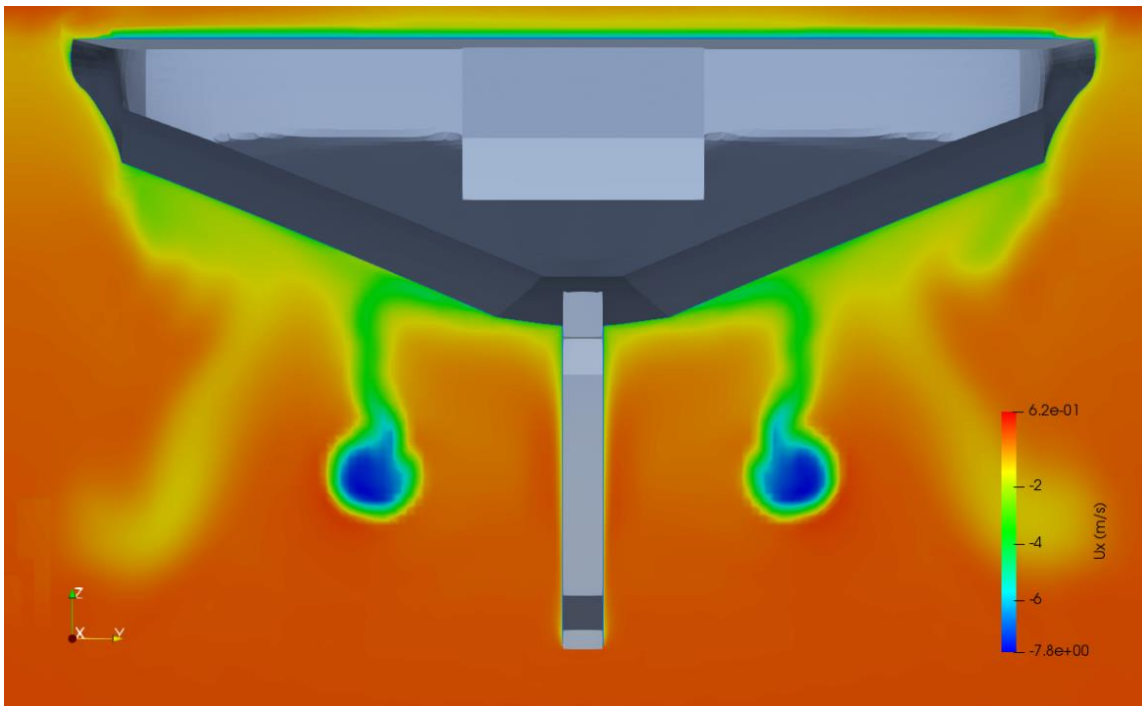
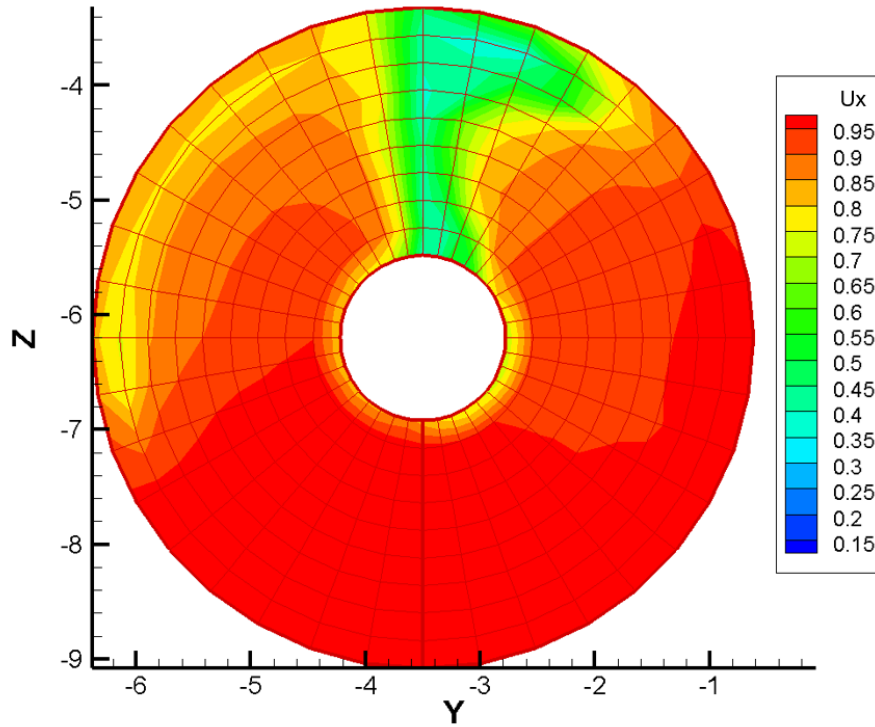


Figure 5-4 CFD-simulated nominal wake field ( $U_x$ : velocity component in the X direction) on the propeller plane as viewed from the aft of the vessel





**Figure 5-5 Effective wake field ( $U_x$ : velocity component in the  $X$  direction, unit m/s) induced by the CCGS *Terry Fox* at a speed of 12 knots, port side propeller plane**

Based on the input effective wake field data, PROCAL was used for numerical simulation of the pressure distribution on the blades and the cavity volume characteristics if applicable. **Figure 5-6** shows the BEM mesh for the propeller blade surfaces and the presumed wake surface for a BEM simulation. It is noted that in this BEM simulation the hull is replaced with the effective wake field, which comes toward the propeller from the left side; the presumed wake needs to extend sufficient far downstream for good simulation quality.

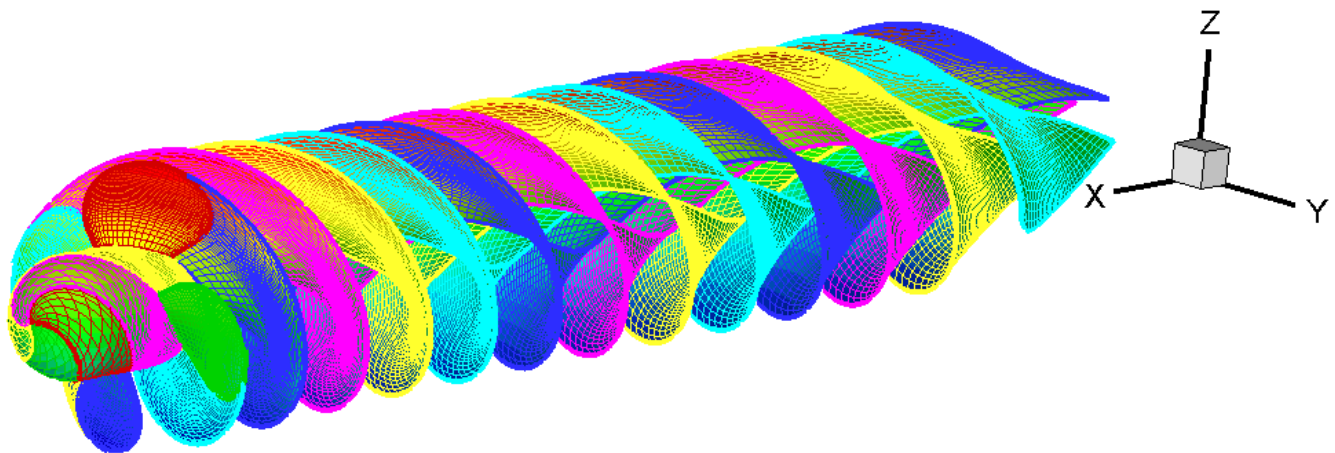


**Figure 5-6 BEM Meshes on the propeller blades, hub, and the presumed wake surfaces for PROCAL simulation**

The PROCAL calculation is based on the unsteady cavitating mode. The cavitation number is estimated as 2.4 for this case. **Figure 5-7** shows the sheet cavities resolved along the leading edge, close to the tip, of the propeller blade at the top dead center. No cavities were found to be existing on the blades at other positions. The small red dot on the leading edge of the top blade but close to the root is a minor cavity which lasted for very short time and hence was considered negligible.

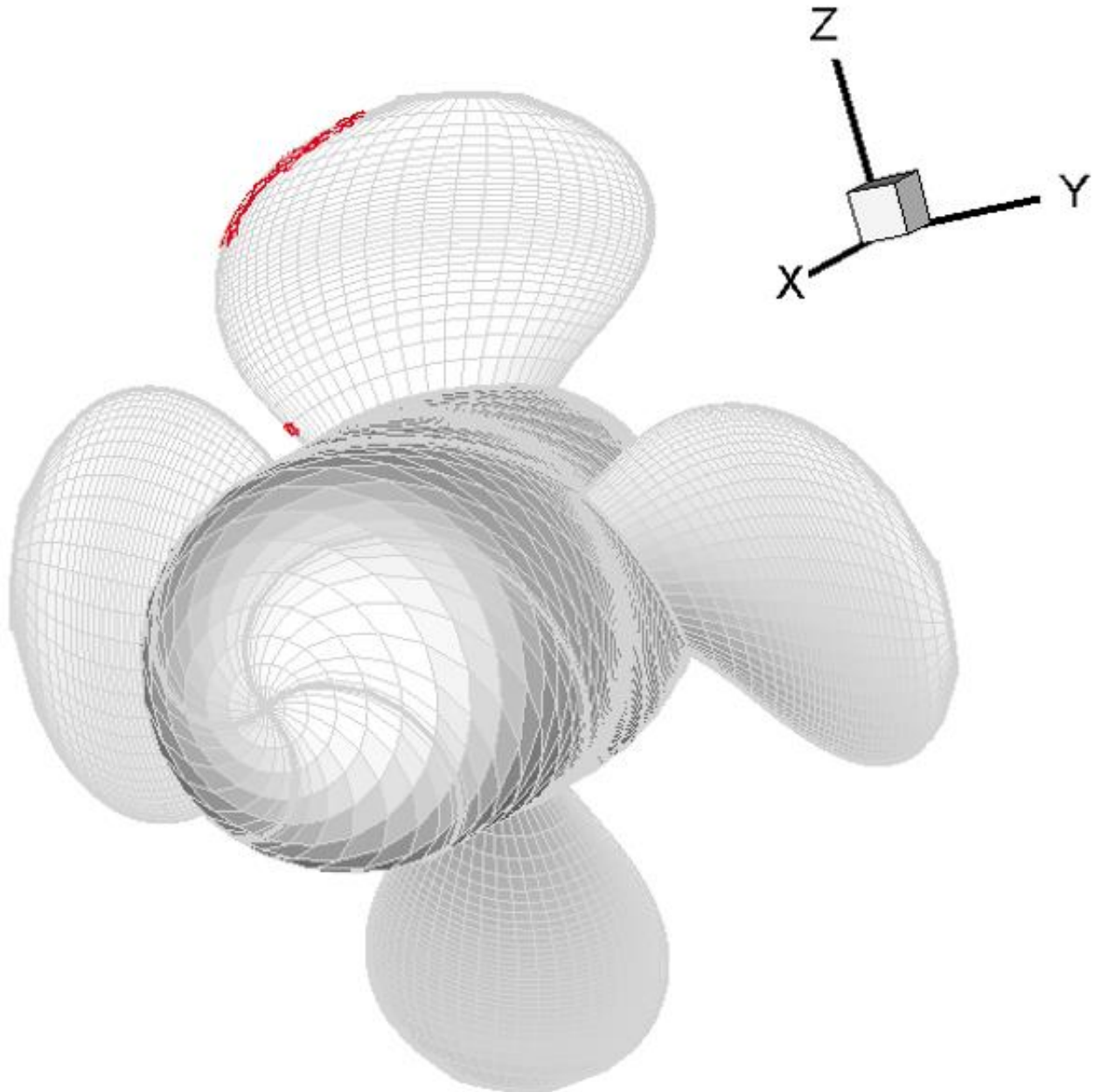


**Figure 5-7 Sheet cavity patterns resolved on the propeller blade surfaces by the BEM-based simulation (propeller RPM 129.7; cavitation number 2.4)**

### 5.3.2 Noise Assessment Using ETV Method For Tip Vortex Cavitation

The ETV-3 tool was used for estimating the impact of the blade tip vortex cavitation on URN. Besides the input from PROCAL, the general information of the vessel and the propeller(s) also needed to be provided. **Figure 5-8** shows an example of the additional information required for the model. The underwater radiated noise levels as predicted by ETV and expressed in the 1/3 octave broadband frequency ranges are shown in **Figure 5-9**. There are two evident spectral peaks in the noise spectrum, one at 8.649 Hz and one at 16.432 Hz, which are the tonals at harmonics of the blade passage frequency (i.e., 8.649 Hz). The impact of the tip vortex cavitation appears to be quite limited (under 160 dB) as predicted by the ETV model.

ETV-model v3.0: PREDICTING BROADBAND PRESSURE LEVELS BY A CAVITATING VORTEX			
Release June 19, 2020		<input type="checkbox"/> HIDE/UNHIDE BOX B-D	
<b>A1: PROPELLER INPUT</b>			
shaft rotation rate	n=	129.7	[rpm]
propeller diameter	D=	4.8	[m]
number of blades	Z=	4	-
number of propellers	Nprop=	2	-
-----			
hull pressure : propeller-hull clearance	Cph=	0.30	[m]
hull pressure: solid boundary factor	SBF=	1.80	-
-----			
URN-LM : shaft submergence	Hshaft=	5.50	[m]
URN-LM : cavity height in propeller disc	H_cav=	0.90	h/R
URN-LM hydrophone depression angle	Theta=	21.56	[deg]
<b>A2: SOURCE LEVEL INPUT MODE</b>			
Input mode for Xkp3 and Xf3	mode=	1/2: Procal	<input type="button" value="▲"/> <input type="button" value="▼"/>
Empirical coefficients	tuning id=	1/4: ONBOARD study	<input type="button" value="▲"/> <input type="button" value="▼"/>
-----			
<u>Mode 1: Procal output for unsteady cavitating flow</u>			
ETV Pressure parameter	XKp3=	8.55	[dB]
ETV Frequency parameter	Xf3=	161.40	-
<b>A3: SPECTRAL SHAPE DEFINITION</b>			
half power bandwidth, sinc hump	b(df)=	0.80	-
upward slope, URN spectrum	a(Ls)=	2.00	-
downward slope, URN spectrum	a(Ls)=	-2.00	-
ΔLs of peak sinc hump and spectrum	ΔL_alfa=	-7.00	dB
peak ratio of sinc hump and spectrum	alfa=	0.80	-
-----			
water density	rho=	1025.0	[kg/m3]
speed of sound	c=	1450	[m/s]
<b>A4: APPLIED ETV PARAMETERS</b>			
Pressure parameter	XKp3=	8.55	[dB]
Frequency parameter	Xf3=	161.40	-
Pressure coefficient a	a(p)=	12.6	[dB]
Pressure coefficient b	b(p)=	1.00	-
Frequency coefficient b	b(f)=	0.24	-

Figure 5-8 Sample input sheet for setting up the ETV-3 model

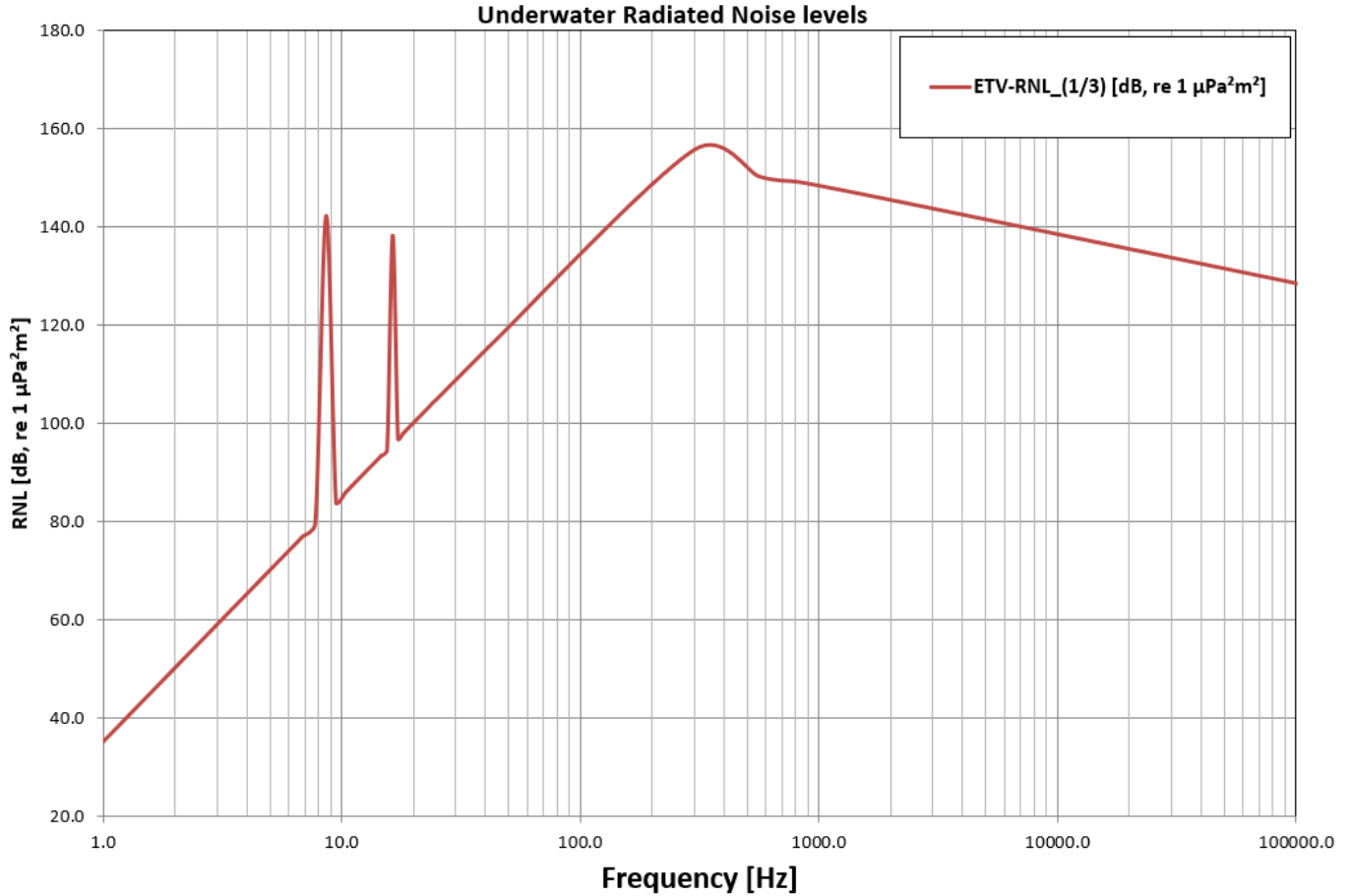


**Figure 5-9 Predicted underwater radiated noise levels as a result of the propeller tip vortex cavitation using the ETV model (in 1/3 octave band)**

### 5.3.3 Noise Assessment Using Dba Method For Sheet Cavitation

As introduced earlier, the dBA tool focuses on the effect of sheet cavitation of the propeller blades on the URN. **Figure 5-10** shows an example of the dBA tool interface. For the *CCGS Terry Fox* in steady state at a speed of 12 knots, the dBA-predicted noise levels are shown in **Figure 5-11** (in terms of 1/3 octave band). Apparently, the dBA-calculated noise levels are much higher than those from the ETV model. This implies that the contribution of sheet cavitation was stronger than that of tip vortex cavitation to the induced URN.

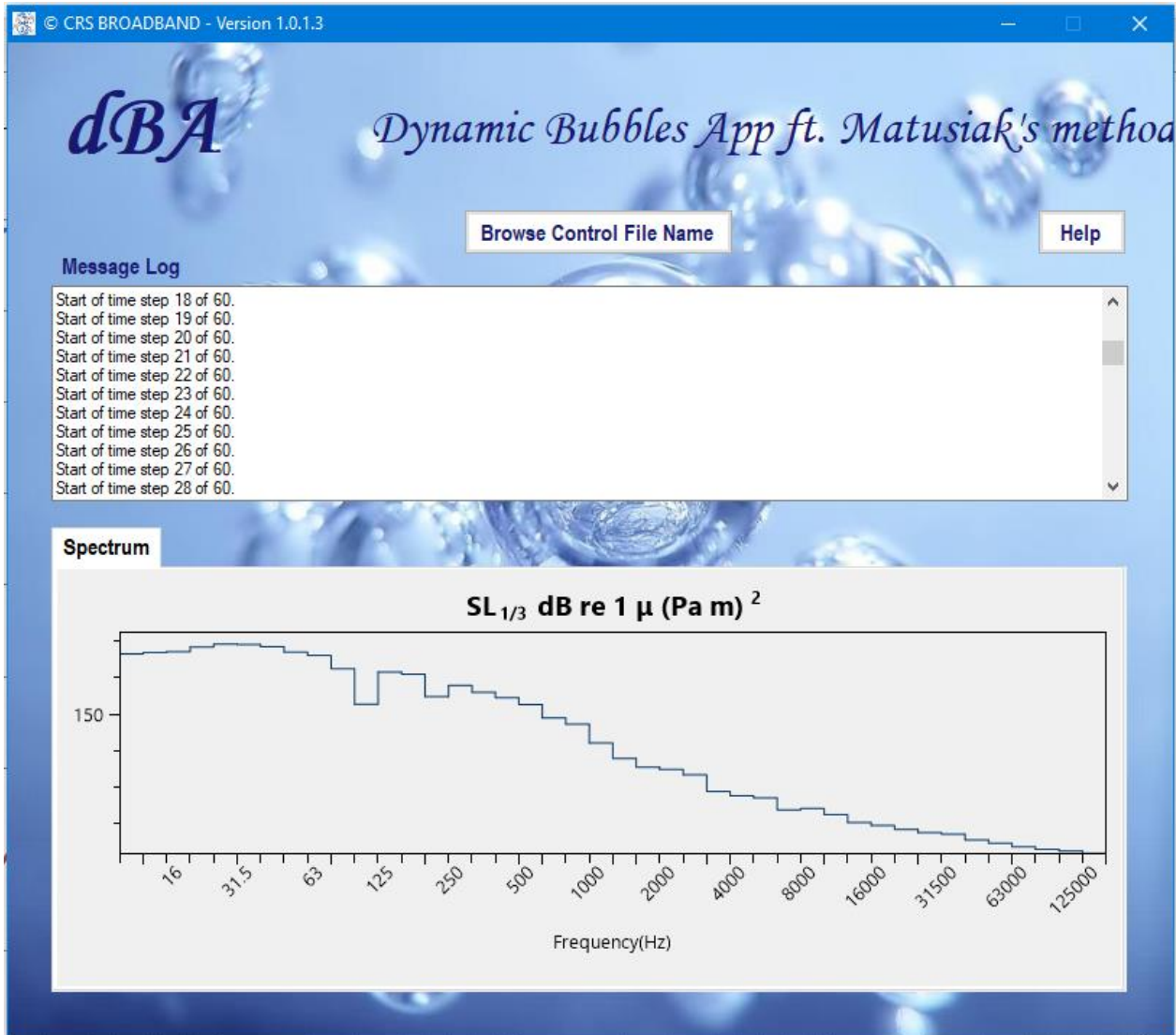
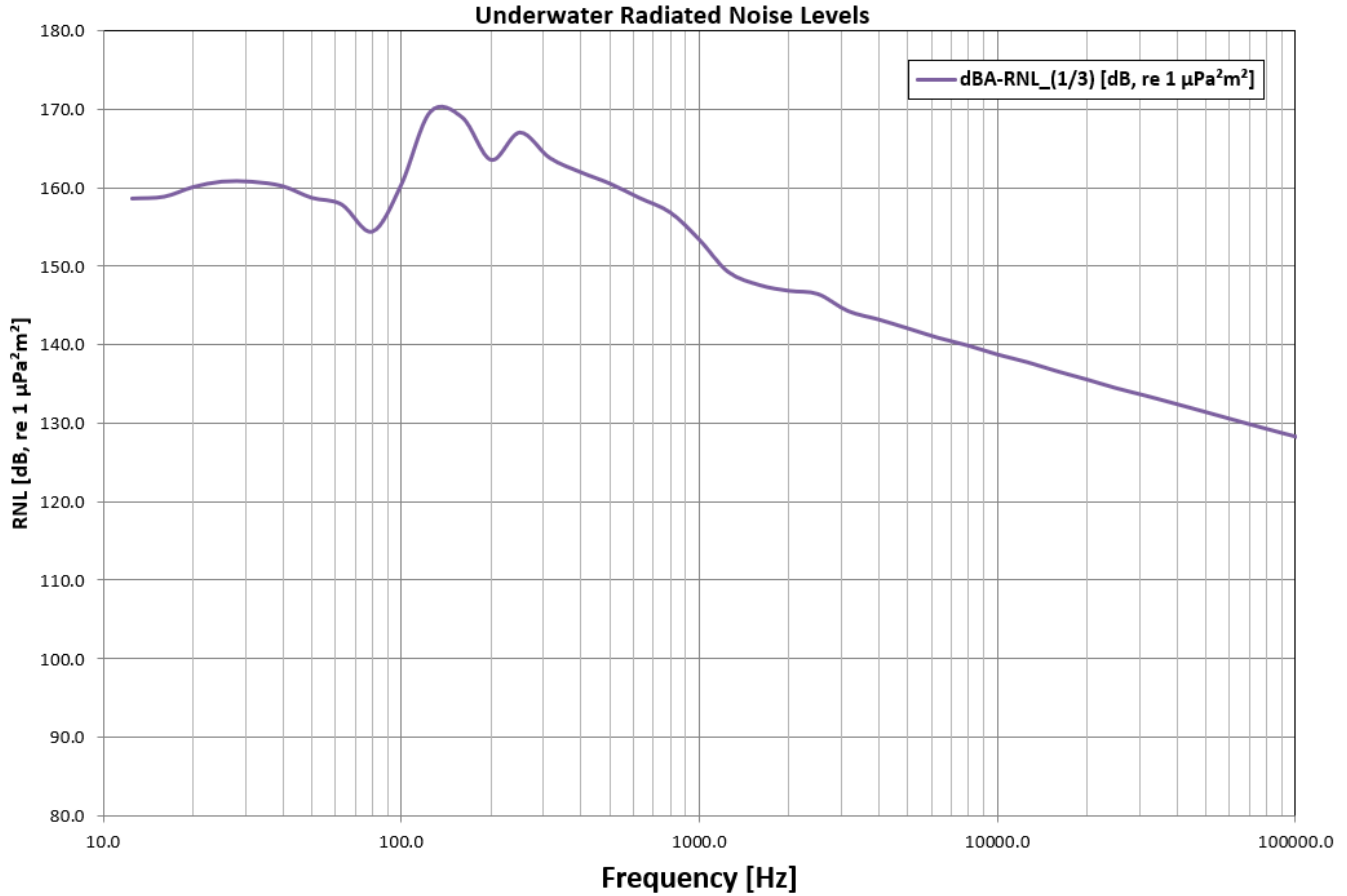


Figure 5-10 Input and output panels of the dBA tool



**Figure 5-11 dBA-predicted underwater radiated noise levels due to sheet cavitation of the subject vessel at a constant speed of 12 knots (in 1/3 octave band)**

### 5.3.4 Combined Noise Levels For The Subject Vessel

The total propeller-induced noise levels, including the influences from both sheet and tip vortex cavitation, was obtained by the logarithmic sum of the separate components from the dBA and the ETV model results, respectively. **Figure 5-12** shows this combined noise spectrum in 1/3 octave bands (blue) along with the sea trial measurements (red). It can be observed, that over the mid-frequency range (i.e., 100 ~ 1000 Hz), the predicted noise levels are in good agreement with the measurement data, with a maximum discrepancy of approximately 5 dB. The difference between the predicted and the measured noise levels becomes larger, i.e., up to 20 dB, at lower and higher frequency ranges. That results from the limitations of the ETV and the dBA models and the BEM-based simulation.

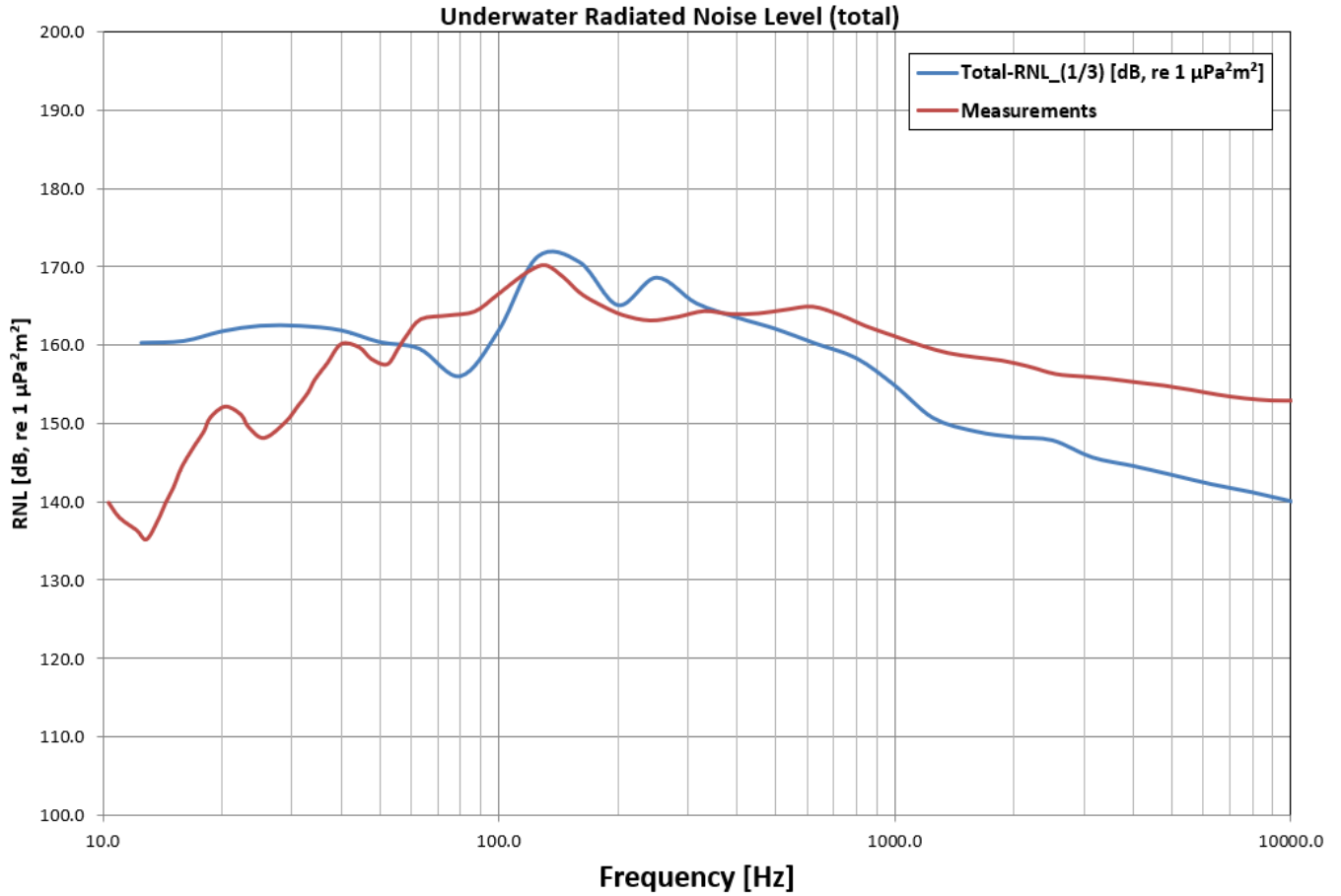


Figure 5-12 The total noise levels resulting from both sheet and tip vortex cavitation (in 1/3 octave band)

## 6 HIGH-FIDELITY URN ASSESSMENT

### 6.1 Methodologies

In practical situations, URN is determined by many factors including the noise from the propeller(s) and that from machinery. This section explores advanced modeling techniques to take the machinery-induced, structure-borne noises into account.

There are two different approaches to computing hydroacoustics: the direct method and the hybrid method. The direct method solves the entire hydroacoustic problem from first principles by assuming the fluid medium to be compressible. The cost of modeling is prohibitive. The hybrid method, instead, features an acoustic analogy, which affords the decoupling of noise generation from propagation. The most classical analogy is based on the inhomogeneous wave equation derived by Lighthill [11], i.e.,

$$\frac{\partial^2 \rho}{\partial t^2} - c_0^2 \frac{\partial^2 \rho}{\partial x_i^2} = \frac{\partial^2 T_{ij}}{\partial x_i \partial x_j} \quad (3.5)$$

with the Lighthill tensor  $T_{ij}$  expressed as

$$T_{ij} = \rho u_i u_j + (p - c_0^2 \rho) \delta_{ij} + \tau_{ij} \quad (3.6)$$

In Eq. (3.5),  $c_0$  is the speed of sound in the medium,  $t$  is the time,  $x_i$  is spatial coordinates,  $\rho$  is the medium density,  $u_i$  and  $u_j$  are the components of the fluid velocity,  $p$  is the pressure,  $\delta_{ij}$  is the Kronecker delta tensor, and  $\tau_{ij}$  is the viscous stress tensor. It allows the calculation of the acoustic propagation from relatively small regions of turbulent flow embedded in a homogeneous fluid. This framework is implemented and expanded in ACTRAN (Hexagon, [12]), where a transformed potential,  $\psi$ , is adopted instead of the medium density as in Eq. (4.1). The following alternative equation as expressed in the frequency domain for the Lighthill analogy is obtained [13]:

$$\frac{\omega^2}{c_0^2} \psi + \frac{\partial^2 \psi}{\partial x_i \partial x_j} = \frac{1}{i\omega} \frac{\partial^2 \tilde{T}_{ij}}{\partial x_i \partial x_j} \quad (3.7)$$

where  $\omega$  is the angular frequency,  $\psi = -\frac{c_0^2 \tilde{p}}{i\omega}$ , and the source term  $\tilde{T}_{ij}$  is related entirely to the momentum components, which are provided by the solution of the flow field.

The present study applies the hybrid method where the flow field is independently computed using a CFD code (i.e., OpenFOAM) and the hydroacoustics is computed using ACTRAN. This method is in fact a one-way interaction between the flow and the acoustic fields. That means the flow field determines the propagation of the acoustic waves, but the acoustic waves have no effect on the flow field. The hybrid method as implemented by ACTRAN has two major steps: a) an interface CFD (referred to as “iCFD”) analysis and b) an acoustic analysis. The iCFD step computes the acoustic sources based on the time-domain CFD solutions. A Fourier transformation is performed to produce the corresponding acoustic source strengths in the frequency domain. These acoustic sources will serve as the boundary conditions



for the second step, i.e., the acoustic analysis. The acoustic analysis then solves the acoustic wave propagation outside of the source zone.

## 6.2 CFD Methodology For The Propeller-Induced Cavitating Flow Field

Full-scale simulation of propeller cavitation behind a vessel is very challenging and requires formidable computational resources. For the present work, ABS chose to conduct the CFD simulation at the model scale first. The scaling factor was 1:26 (so the length scaling factor  $\lambda_L = 26$ ). OpenFOAM was used as the CFD analysis package. The k- $\epsilon$  turbulence model with wall functions was used to resolve the turbulent boundary layers over the hull and propeller surfaces. To further simplify the CFD model, only the aftbody of the hull was included in the simulation. The CFD model was based on a double-body setup, where no free-surface effect was considered. The AMI (Arbitrary Mesh Interface) method was adopted for handling the connection of the rotating grid domain around the propeller with the hull grid domain. The AMI, as implemented in OpenFOAM [14], is particularly efficient for rotor machinery applications, such as turbines and marine propellers. The OpenFOAM solver, “interPhaseChangeDyMFoam”, was adopted for simulating cavitation. This solver was developed based on a cavitation model, the Schnerr-Sauer model, whose model coefficients are more robust than those of other candidate models for cavitation simulations. For a general cavitation prediction, the use of advanced turbulence models such as Large Eddy Simulation is typically recommended. However, since cavitation-induced noise is believed to dominate the ship-induced noise as in the present case, a Reynolds-Averaged Navier-Stokes (RANS) based CFD model suffices. The RANS modeling framework preserves the power to provide propeller-induced loads for noise generation. At the same time, the RANS model could seriously smear the fine eddy structures in the turbulent flow. This would lead to a loss of the turbulence-induced noise, which is just a minor part of the total noise for a vessel moving with cavitating propellers. For the model-scale CFD simulation, ABS had the liberty to choose a vessel speed. For convenience, the same speed of 12 knots was assumed. The time step was chosen as 0.001 s.

The cavitation number  $\sigma$  is estimated to be 2.403 at full scale, based on a characteristic velocity of 12 knots. ABS adopted a propeller rotational speed of 36 RPS (revolutions per second, denoted as  $n$ ) for the model-scale CFD simulation. According to the scaling similitude for cavitation number and advance coefficient ( $J$ ) of the propeller [15], the following scaling relations are adopted:

$$\sigma_S = \frac{P_S - P_{VS}}{\frac{1}{2}\rho_S V_{RS}^2} = \sigma_M = \frac{P_M - P_{VM}}{\frac{1}{2}\rho_M V_{RM}^2} \quad (3.8)$$

$$J_S = \frac{V_S}{n_S D_S} = J_M = \frac{V_M}{n_M D_M} \quad (3.9)$$

where the subscript  $S$  is for the full-scale (ship) values, and the subscript  $M$  is for the model-scale values. Also, in the above equations (3.8) and (3.9),  $D$  is the propeller diameter;  $V_R$  is the reference velocity; and  $P_V$  is the saturation pressure of water.

Therefore, the velocity and time scaling factors for this problem are:

$$\lambda_V = 1.562$$

$$\lambda_T = 16.65$$

The scaling relationship for pressure, between  $P_S$  and  $P_M$ , is:

$$P_S = \lambda_V^2(P_M - P_{VM}) + P_{VS} \tag{3.10}$$

where  $P_{VS} = P_{VM}$  is the saturation pressure of water.

Once the model-scale CFD simulation is completed, the flow parameters were converted to full scale using the scaling factors as described above.

### 6.3 CFD simulation results

All results presented here have been converted to the full scale. **Figure 6-1(a)** shows a cut-away view of the volume mesh in a vertical plane across the propeller shaft. The mesh in the region near the propeller was refined for capturing the complex flow such as the tip and the hub vortices. **Figure 6-1(b)** shows a subdomain defined in the CFD computational domain where the flow data generated by CFD were exported for the ACTRAN model. This subdomain was set to encompass the key flow patterns around the propeller that would be critical for noise generation. The small cylindrical region inside the subdomain is the shade of the AMI domain. It should be noted that such flow data were time-varying.

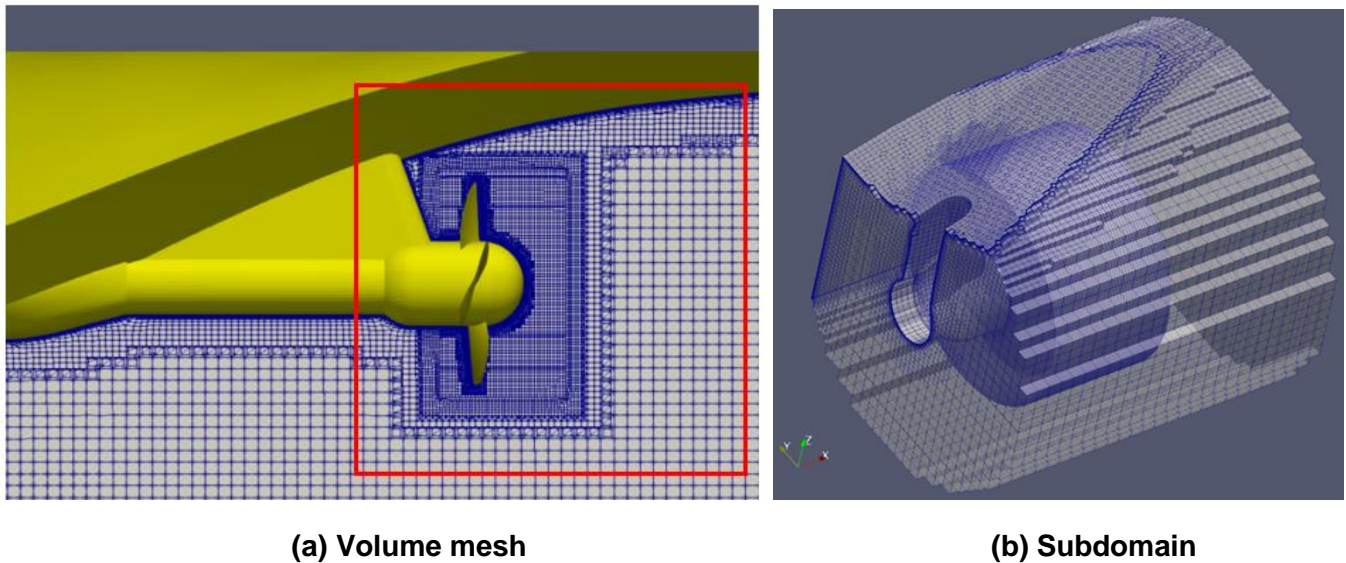


**Figure 6-1 (a) CFD computational mesh in the vertical plane across the propeller shaft; (b) a subdomain used for flow field data sharing for the acoustic analysis using ACTRAN**

**Figure 6-2** shows the distribution of the longitudinal velocity component,  $U_x$ , in the vertical plane crossing the propeller shaft on the portside. The CFD simulation appeared to have successfully captured the accelerating flow across the propeller plane.

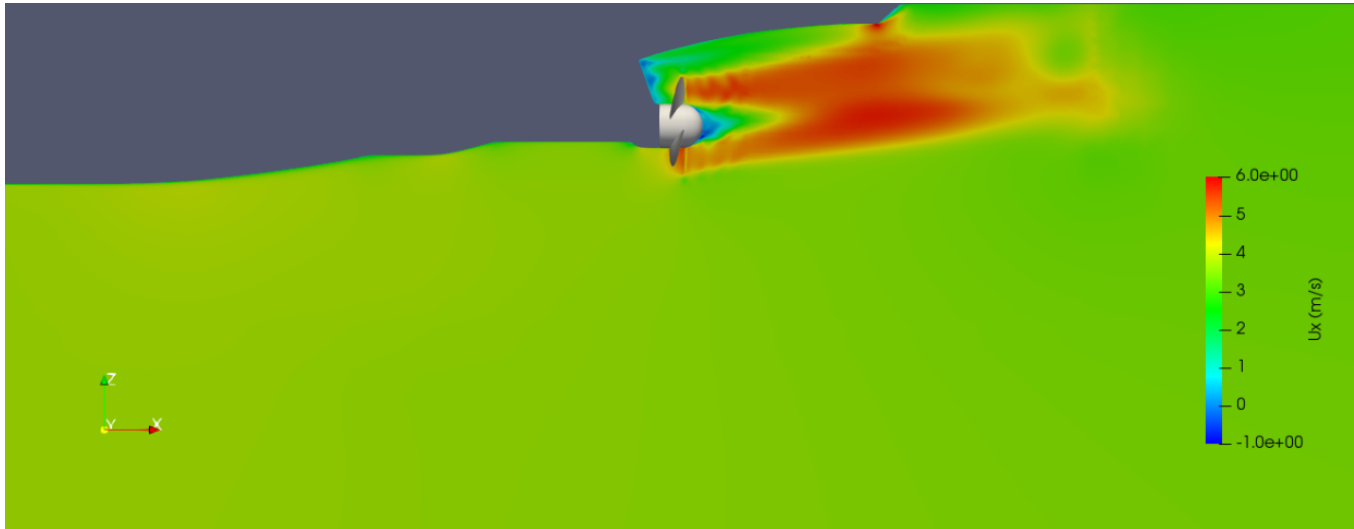


**Figure 6-2 Distribution of the longitudinal velocity component  $U_x$  in the vertical plane crossing the propeller shaft**

**Figure 6-3** shows the sheet cavity pattern along the propeller blades. Like the results from the PROCAL simulation, the cavity appeared around the same position along the leading edge of the blade at the top dead center. There is also a minor cavity on the blade root area, which is also consistent with what PROCAL simulation identified (**Figure 6-3**). **Figure 6-4** shows the pressure distributions on the face side and back side of the propeller.

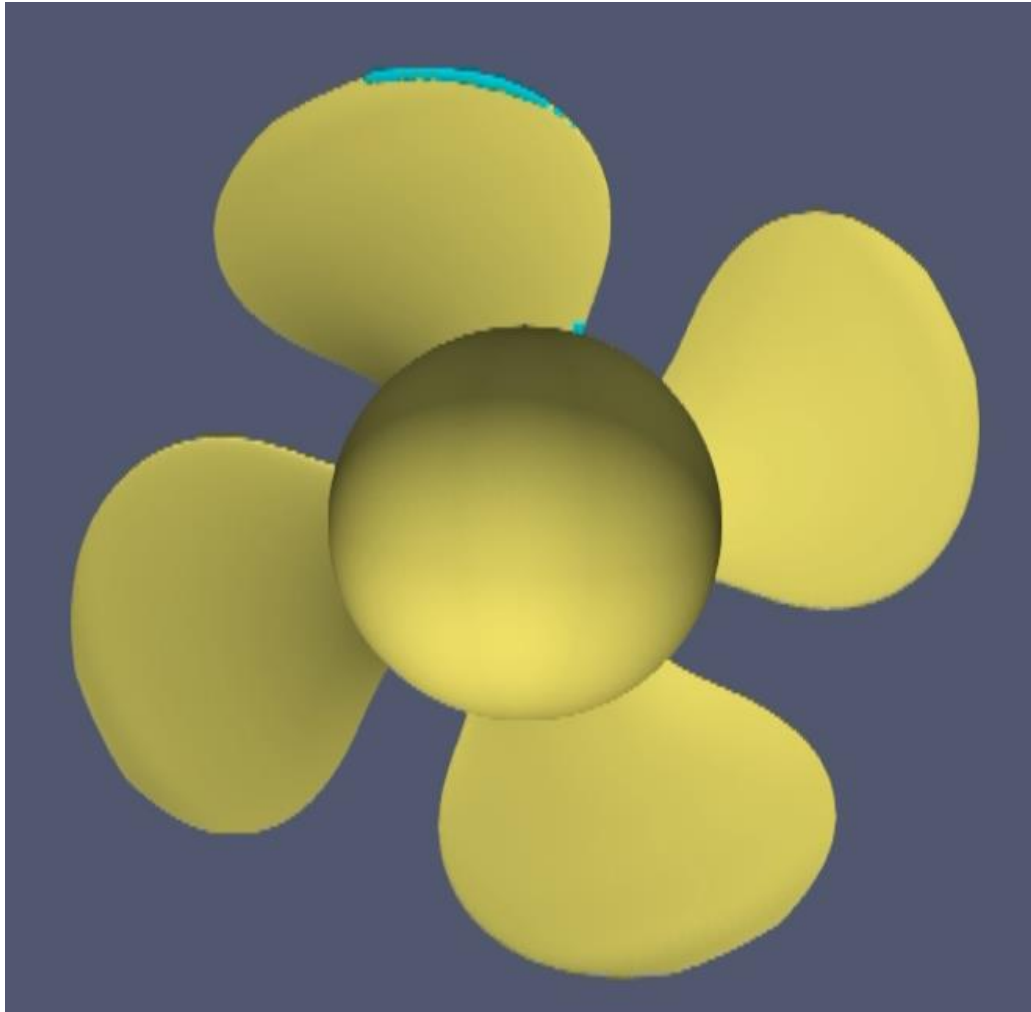
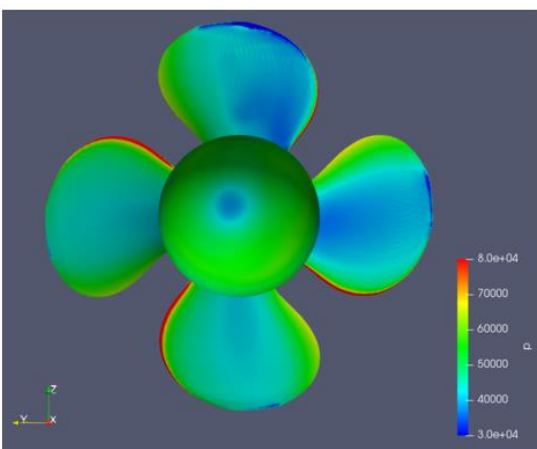
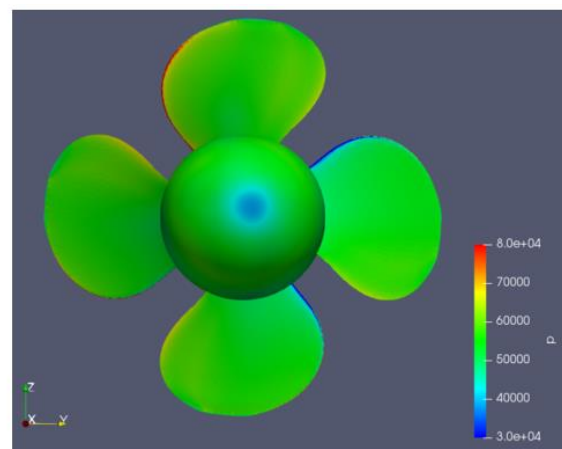


Figure 6-3 CFD-simulated sheet cavity pattern on the blade surfaces



(a) Back side



(b) face side

Figure 6-4 Pressure distributions on the propeller blade surfaces: (a) back side; (b) face side

**Figure 6-5** shows the iso-surfaces of the Q-criterion at two different levels, i.e., 15,000 and 2,000, respectively. These Q-criterion surfaces are suitable for revealing the complex three-dimensional vortical structures as induced by the rotating propeller. The spiral pattern of the tip vortex and the cylindrical pattern of the hub vortex are clearly resolved. The fine vortical structures along blade surfaces, perhaps due to the near-wall shearing, are also resolved. It is important to note that even though the tip vortex was well resolved here no trace of tip vortex cavity was detected (**Figure 6-5**). This implies that the tip vortex was somehow in a wetted condition instead of cavitating.

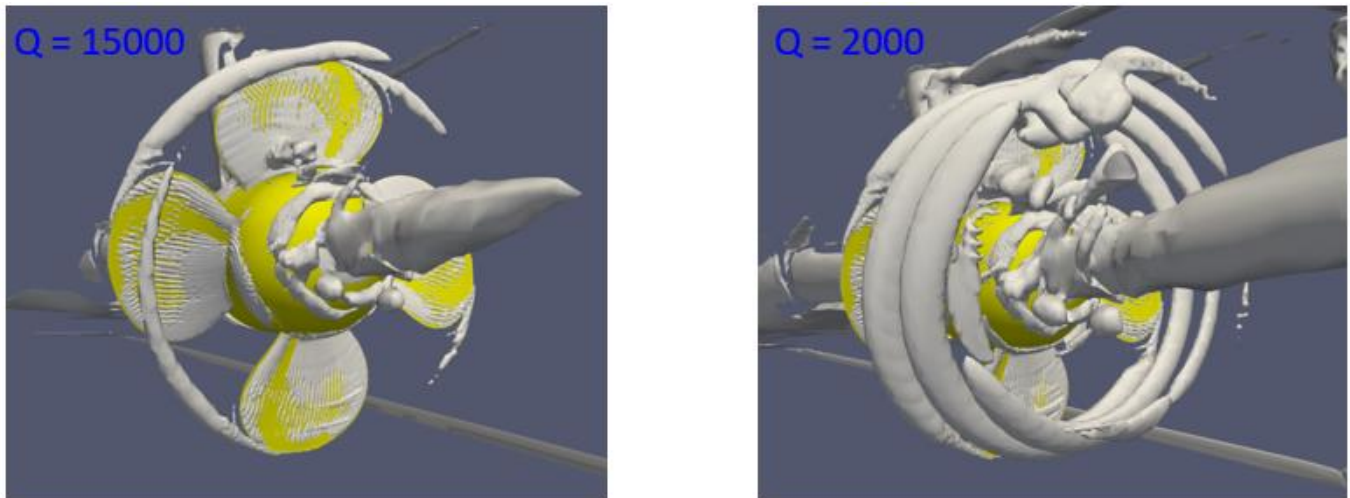


**Figure 6-5 Iso-surfaces of the Q-criterion at two different levels (left: Q-criterion at 15,000; right: Q-criterion at 2,000)**

**Figure 6-6** shows the distributions of the total pressure and the longitudinal velocity component  $U_x$  in the subdomain for data sharing. The velocity and pressure fields along with the mesh information inside the subdomain were exported into data files in the Enight format for every time step to be used by ACTRAN.

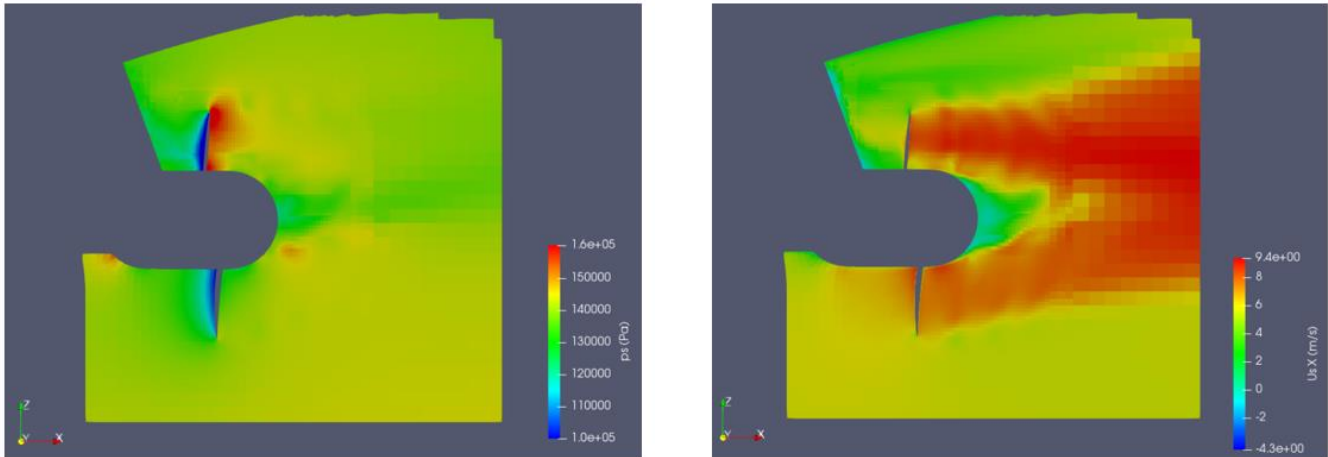


**Figure 6-6 Distributions of the full-scale total pressure and the full-scale velocity component  $U_x$  in the subdomain for data sharing (left: total pressure; right: velocity component  $U_x$ )**

## 6.4 Acoustic Model Setup

### 6.4.1 Acoustic computational domain

The acoustic model as implemented by ACTRAN is based on the Finite Element (FE) method. Since the *CCGS Terry Fox* is a twin-skeg vessel, the induced acoustic field was assumed to be symmetric. Hence, only half of the vessel (i.e., the portside) was represented by the model.

The acoustic computational domain is shown in **Figure 6-7**. The domain is comprised of a finite fluid component (i.e., the near field), which is shown in blue, and a perfectly matched layer (PML) (i.e., the far field), shown in green, aiming to dampen the acoustic waves propagating outward. In this setup, we focus mainly on the near field. The side length of the finite fluid domain was 200 m. The width of the PML was another 100 m. The water depth was set to 200 m to reflect the actual sea trial conditions.

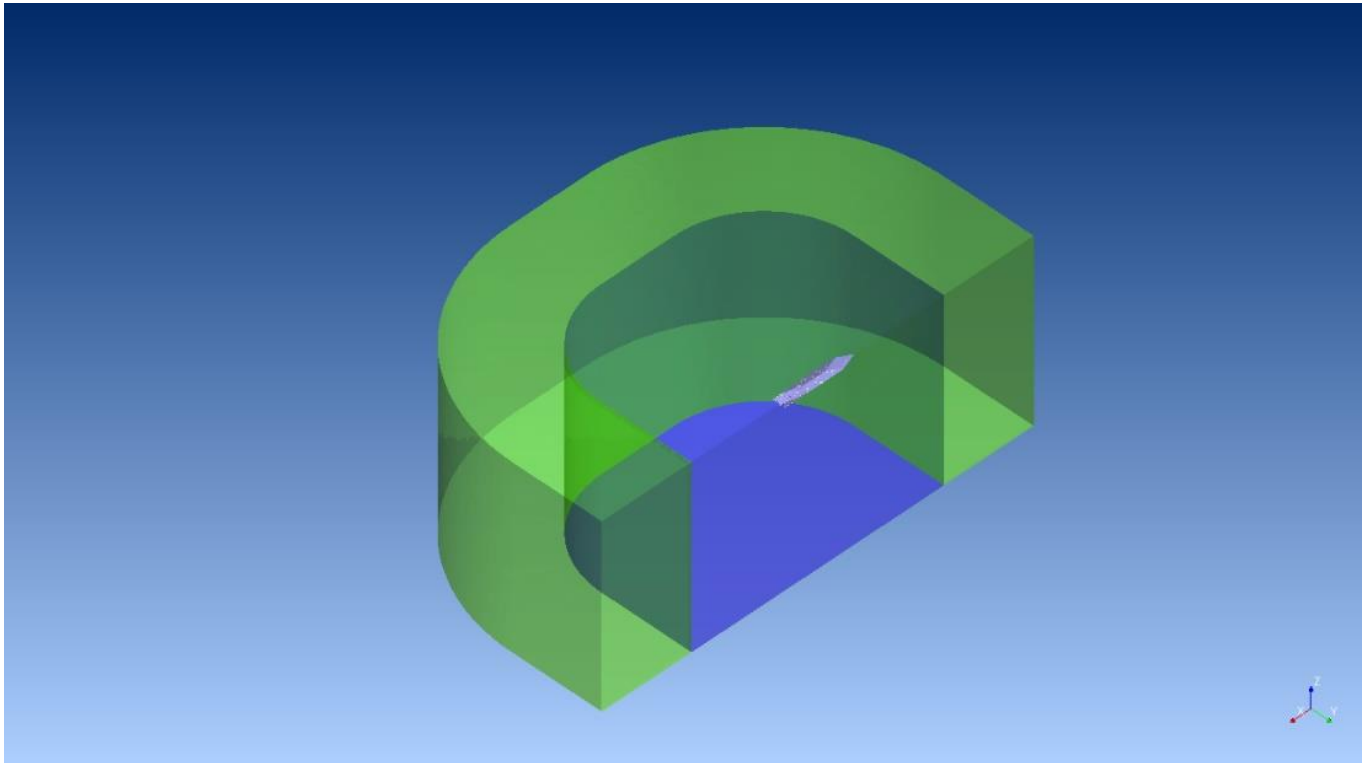


**Figure 6-7 Domain setup for the acoustic analysis using ACTRAN: the finite fluid component (blue) and the PML component (green)**

An FE mesh was generated for the Direct Frequency Response (DFR) analysis, which was used to calculate the frequency-domain response of an acoustic system to an excitation at specific frequencies. The standard meshing criterion was to ensure 4 to 10 linear elements per wavelength of space. A noise radiation problem often engages an unbounded computational domain with infinite elements, which serve as a non-reflective boundary. For the present study, the PML used was an alternative to the infinite elements. The acoustic waves can be transmitted with no disturbance from the finite fluid component into the PML component through the compatible mesh between them.

#### 6.4.2 Boundary conditions for acoustic analysis

The seabed (the bottom of the domain) was treated as a solid wall. Three other types of boundary conditions were imposed (Figure 6-8 ): a zero-pressure boundary condition (blue) was set for the water surface. This setting means to fully reflect all incident acoustic waves but with a 180° phase shift. A non-reflecting boundary condition (green) was applied on the outside of PML region. The vessel center plane was imposed a symmetric boundary condition (red), where a zero acoustic normal acceleration was implemented. To take the propeller loading into consideration, a Lighthill surface boundary condition was applied on a cylindrical surface as shown by the yellow surface in Figure 6-9 . This cylindrical surface coincides with the export subdomain from the CFD model (**Figure 6-7**).

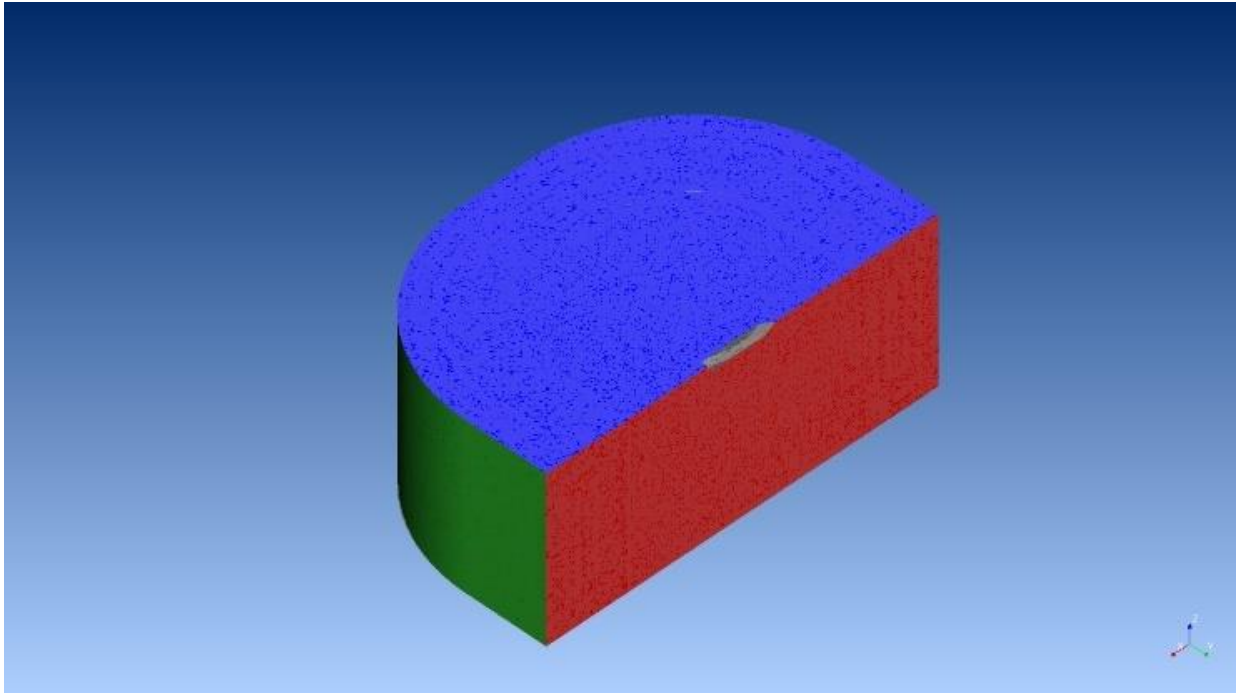


**Figure 6-8** Boundary conditions of the acoustic model. The red color indicates a symmetric boundary; the blue color indicates a zero-pressure boundary; the green color indicates a non-reflecting boundary. The vessel center plane (red) is at  $Y = 0$ . The top plane (blue) is at  $Z = 0$

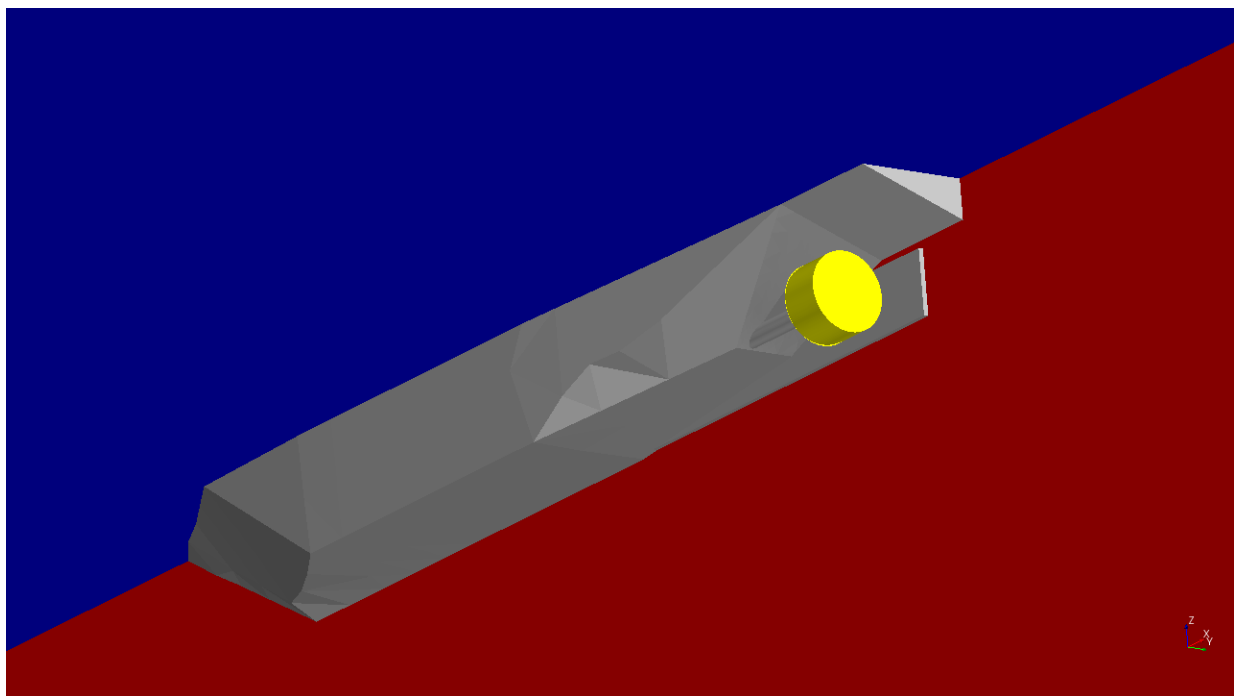


**Figure 6-9** Implementation of the Lighthill surface boundary condition on the yellow cylindrical surface of the acoustic model



### 6.4.3 Placement of the numerical hydrophones

Three numerical hydrophones were used to capture the sound pressure level (SPL) in the acoustic field. The transverse distances (i.e., 180 m from the vessel centerline) and depths (i.e., 32, 64 and 96 m, respectively) of the hydrophones, as depicted in **Figure 6-10** , are consistent with the three actual hydrophones used for the sea trial. Longitudinally, the hydrophones are in the same plane going through the propeller center. This configuration reflects the instant when the vessel passed by the actual hydrophones in the sea trial and the point above the hydrophones on the water surface is the Closest Point of Approach (CPA) for delineating the vessel noise signature.. The detailed coordinates of the hydrophones in the acoustic model are listed in Table 6.1. The origin of the coordinate system is at the ship bow, as indicated by the red point in **Figure 6-10** .

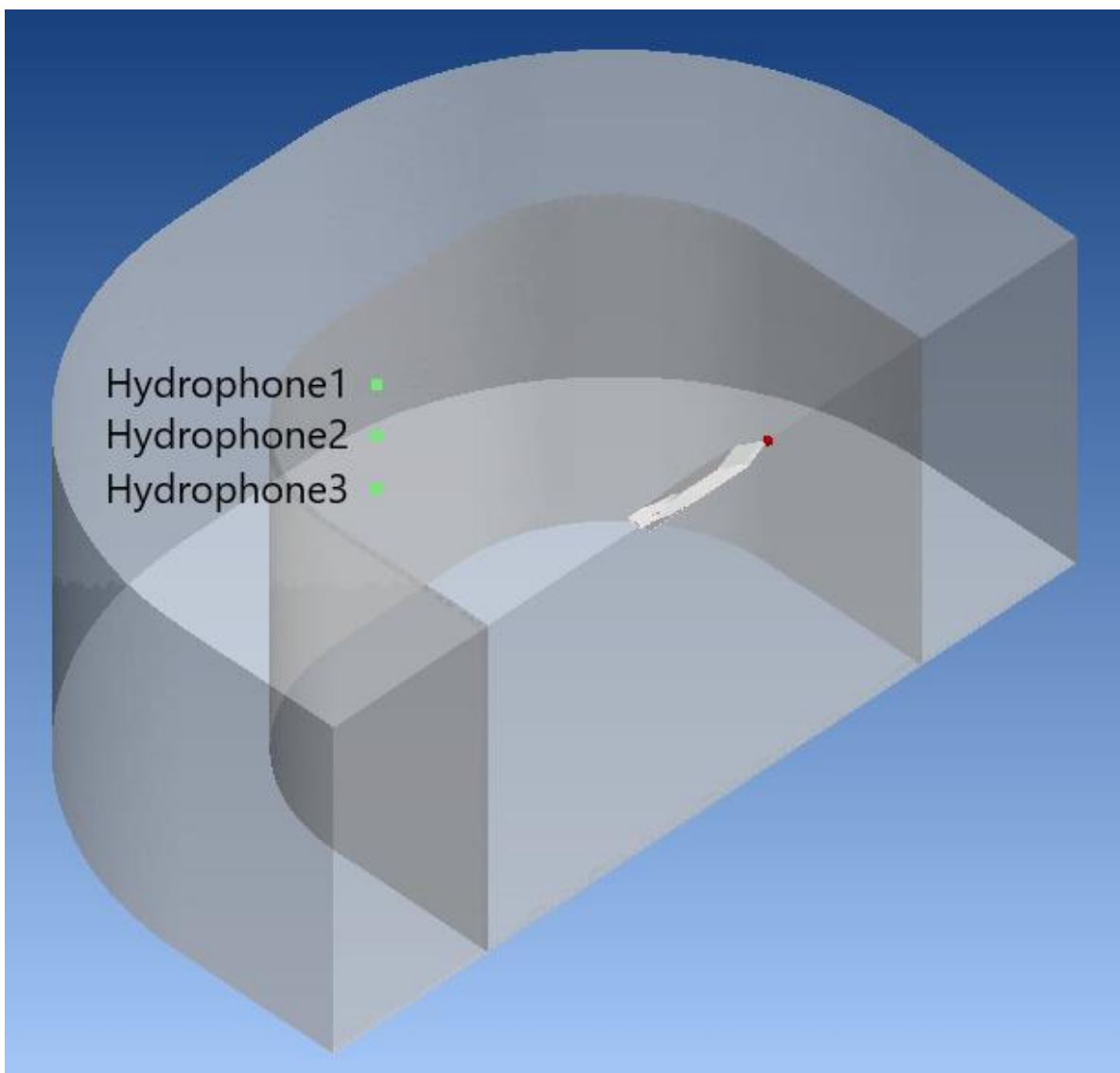


**Figure 6-10 Numerical hydrophone locations in the acoustic model. The red point indicates the origin of the coordinate system**

**Table 6.1 Coordinates of the three numerical hydrophones**

No.	X (m)	Y (m)	Z (m)
1	73.3	180	32
2	73.3	180	64
3	73.3	180	96

#### 6.4.4 Results of iCFD Analysis

The iCFD analysis was carried out to compute acoustic sources, i.e., the Lighthill surface sources, on a pre-defined surface surrounding the propeller blades. Ideally, this source surface should be as close to the blade surfaces as possible. For simplicity, a small cylindrical surface surrounding the propeller blades was adopted for this purpose. This Lighthill surface is within the CFD subdomain used for data sharing such that the flow parameters from the CFD simulation (Section 3.3.3) can provide sufficient input. A Fourier transform was used to convert the time-domain flow field data into the frequency domain. The relation between the CFD sampling (i.e., the time step that the CFD simulation used,  $\Delta t$ ) and the allowed frequency range for acoustic analysis is:

$$f_{max} = \frac{1}{2 \cdot \Delta t} \quad (3.11)$$

$$f_{min} = \frac{1}{T} \quad (3.12)$$

where,  $f_{min}$  and  $f_{max}$  are the minimum and maximum frequencies one can reach in the acoustic analysis based on the input from the CFD results and  $T$  denotes the time duration of the CFD results. Based on the CFD simulation, the minimum and maximum frequencies for the acoustic analysis are 1 and 300 Hz, respectively. Although the cavitation-induced noise can typically reach a frequency as high as tens of thousands of Hz, it is not feasible to model the high-end of the noise spectrum using high-fidelity modeling.

Figure 6-11 presents some sample results from the iCFD analysis, i.e., the conversion of propeller loading data from the CFD simulation into the frequency-domain Lighthill surface sources.

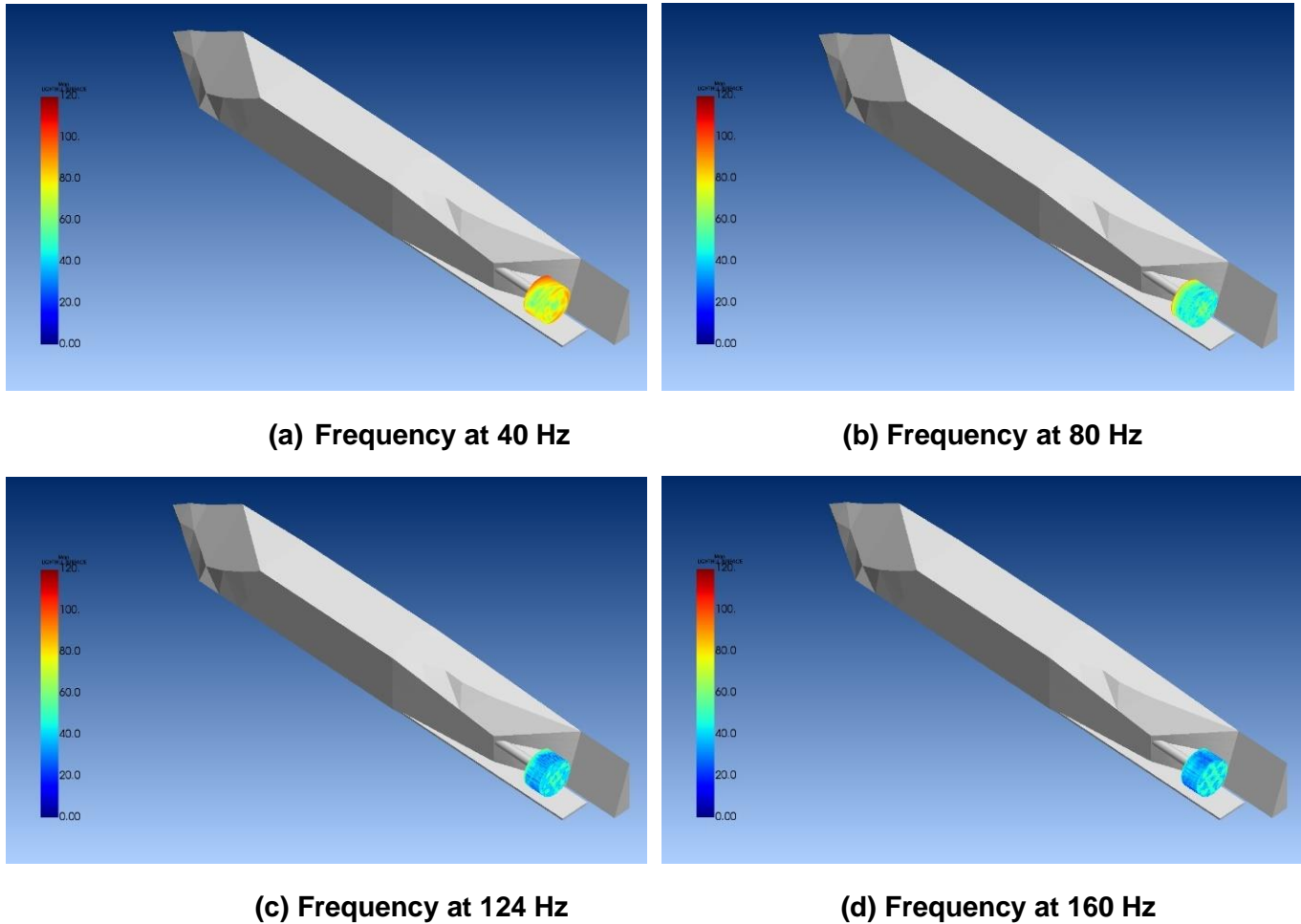
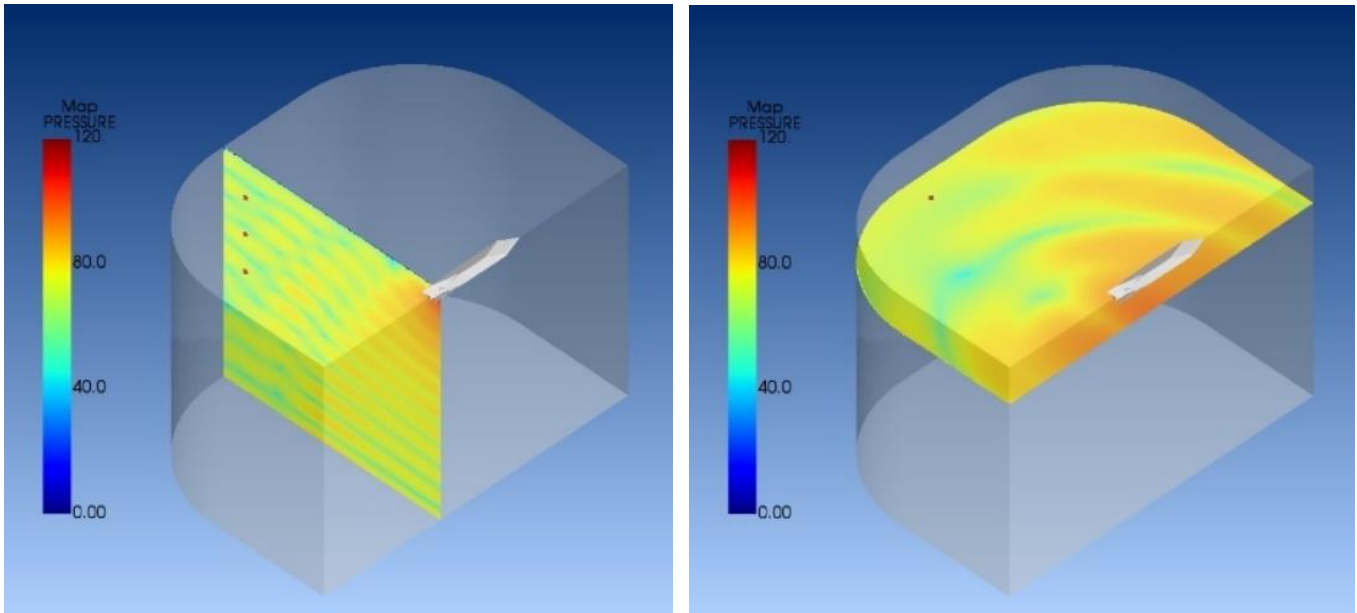


Figure 6-11 Lighthill surface source patterns at frequencies of 40, 80, 124, and 160 Hz

### 6.5 Results of acoustic analysis

The resulting SPL at various frequencies, as viewed in both vertical and horizontal planes, are displayed in Figure 6-12 to Figure 6-14. The vertical cut plan is at  $X = 73.3$  m. The horizontal cut plane is at the same elevation as the top hydrophone. The acoustic wave propagation patterns clearly show that the propeller is the primary source of noise (Figures 3.26 and 3.27). The wave reflection and interference patterns along the free surface and the seabed are also reasonably represented. The acoustic patterns show diffraction and scattering at low frequencies (e.g., at 40 Hz) due to the obstruction of the vessel hull and the appendages. In contrast, the wave patterns at higher frequencies, such as 80 and 160 Hz, appear to be more homogeneous.



**Figure 6-12** Predicted sound pressure level at a frequency of 40 Hz. The pressure unit is dB. The vertical cut plane is at  $X = 73.3$  m. The horizontal cut plane is at  $Z = -32$  m.

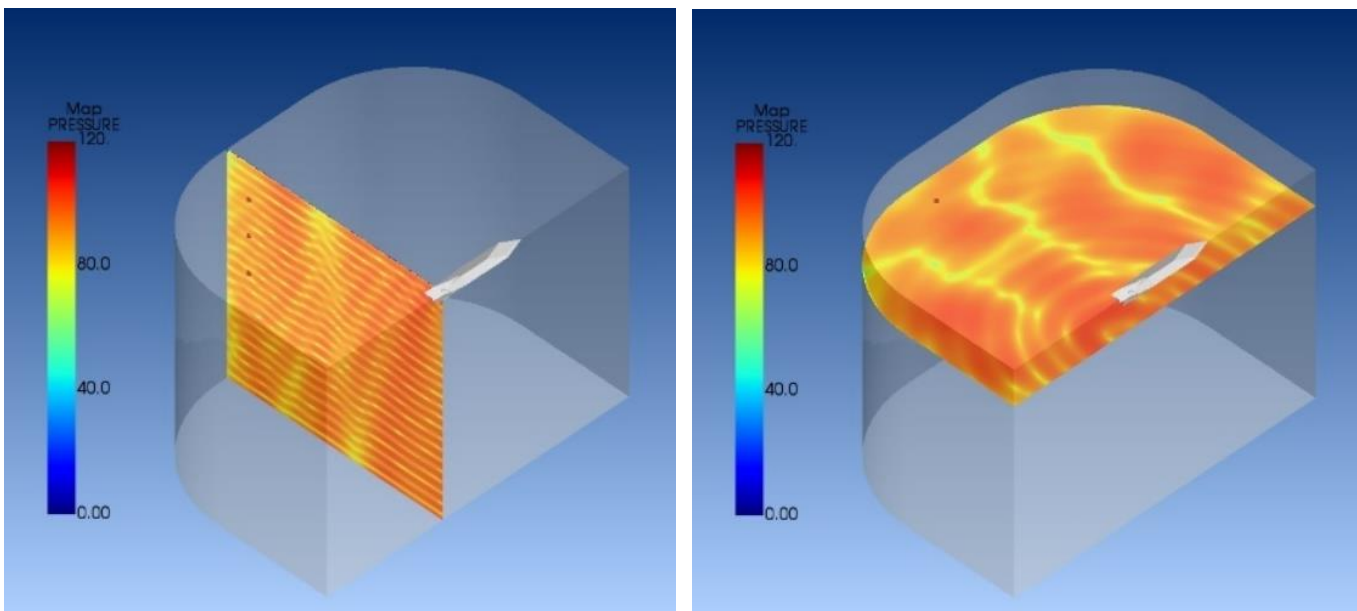


**Figure 6-13** Predicted sound pressure level at a frequency of 80 Hz. The pressure unit is dB. The vertical cut plane is at  $X = 73.3$  m. The horizontal cut plane is at  $Z = -32$  m.

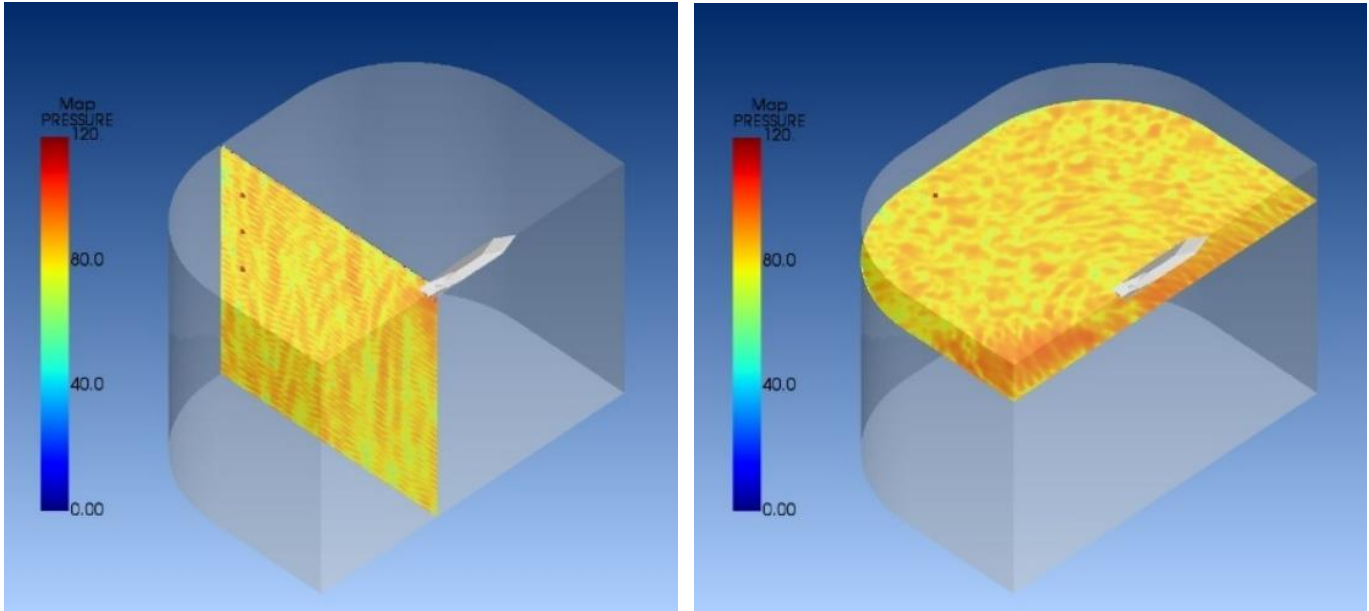


**Figure 6-14 Predicted sound pressure level at a frequency of 160 Hz. The pressure unit is dB. The vertical cut plane is at X = 73.3 m. The horizontal cut plane is at Z = -32 m**

The *RNL* as estimated based on the SPL at each hydrophone was calculated by taking the transmission loss over distance into account (Eq. (3.1)). Figure 6-15 shows the resulting *RNL* (at 1 m distance from the acoustic source) as expressed in the 1/3 octave bands. The *RNL* measured from the portside hydrophones during the sea trial is also shown for comparison. The simulated *RNL*'s agree well with the measured *RNL*'s for the frequencies below 100 Hz. This frequency range is known to be dominated by propeller loads and machinery-induced noises. On the other hand, the acoustic analysis seemed to underpredict the *RNL* for higher frequencies (i.e., between 100 and 300 Hz). The discrepancy could be up to 15 dB. More discussion is provided in a later section.

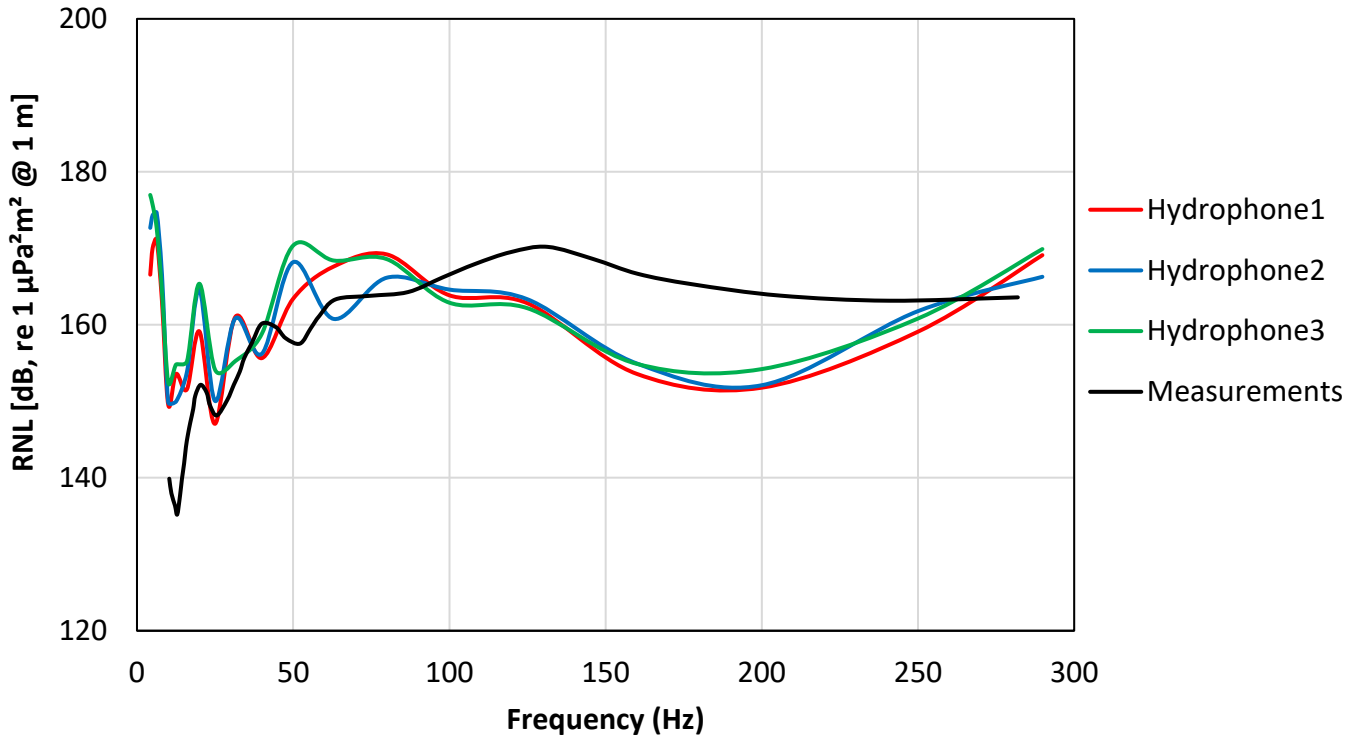


**Figure 6-15 Predicted RNL based on SPL at each hydrophone compared with the RNL from the sea trial measurements**

### 6.6 Machinery-induced URN

In this section, two acoustic software tools, Designer NOISE (developed by Noise Control Engineering, LLC) and ACTRAN, were utilized to calculate the machinery-induced URN. A methodology for machinery induced underwater noise calculation was developed and applied to the subject vessel. The machinery-induced underwater noise was calculated via three stages. The first stage was to calculate the hull vibration level induced by the machinery equipment. The second stage was to calculate the propagated sound pressure levels at the hydrophone locations. The third stage was to calculate the machinery-induced source level of the vessel by considering the transmission loss and averaging the results over all hydrophones.

### 6.6.1 Stage one

In the first stage, Designer NOISE is used to calculate the machinery-induced hull vibration. The software calculates the structure-borne noise spreading throughout the vessel based on hybrid statistical energy analysis (SEA) method. The main hull structures are modeled where all the primary structures are included. Major machinery sources are evaluated in the analysis, such as the main engines. The hull is divided into several subsystems as shown in **Figure 6-16**. The average vibration acceleration level of each subsystem of the hull is calculated and was used as the excitation input for stage two of the analysis.

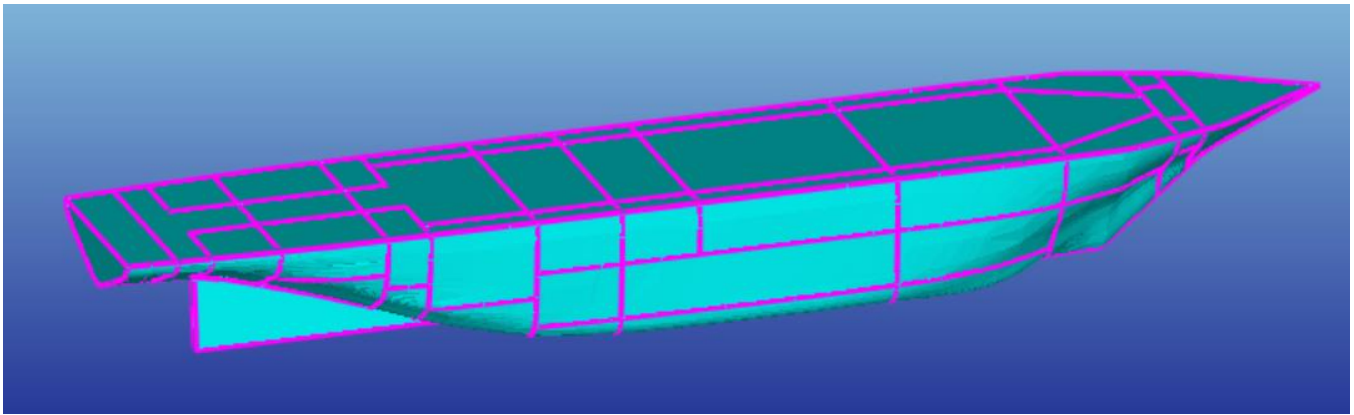


**Figure 6-16 Subsystem Division of the Hull in Designer NOISE**

The SEA method [16] was originally developed to analyze the response of large complex aerospace systems. It calculates the diffusion of acoustic and vibration energy in the complex acoustic system using energy flow relationships. SEA is efficient to deal with the acoustic issues of complex structures at high frequencies, which is difficult to analyze by classical methods. It helps predict the average response of the structure, which avoids a large quantity of calculation and makes it competitive in high frequency analysis of large structures.

In the SEA method, the entire structure is regarded as a system and is divided into several coupled subsystems, such as plates, beams and cavities. Each subsystem represents a store of energy. Under steady-state conditions, a subsystem gains the time-average power from external sources and other connected subsystems. The gained power is taken to be equal to the sum of the power dissipated within the subsystem by damping and the power transmitted to the connected subsystems, which is expressed as

$$P_d = c_v \dot{x}^2 = 2\zeta\omega_n m \dot{x}^2 = 2\zeta\omega_n E = \frac{\omega_n E}{Q} = \omega_n \eta E \quad (3.13)$$

where  $P_d$  denotes the dissipation of energy,  $c_v$  denotes the viscous-damping coefficient,  $\zeta$  denotes the damping ratio,  $\omega_n$  denotes the natural frequency of the system,  $Q$  denotes a quality factor, and  $E$  is the average energy of the subsystem. An example of two coupling subsystems is shown in Figure 6-17 .

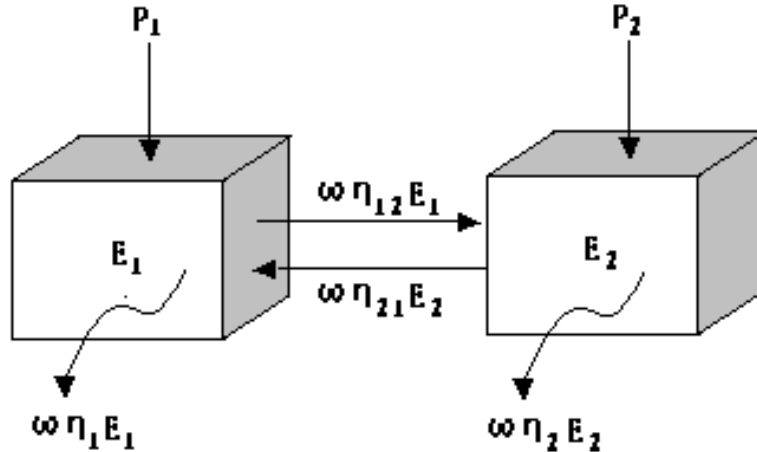


Figure 6-17 Acoustical Power Flow between Subsystems as in the SEA framework

The equations below, for example, describe the basic relationships of the energy flow of the two couple subsystems:

$$\begin{cases} P_{12} = \omega \eta_{12} E_1 \\ P_{21} = \omega \eta_{21} E_2 \\ P_{1,diss} = \omega \eta_1 E_1 \\ P_{2,diss} = \omega \eta_2 E_2 \\ \eta_1 \eta_{12} = \eta_2 \eta_{21} \end{cases} \quad (3.14)$$

where  $P_{ij}$  ( $i, j = 1, 2$ ) denotes the power transmit from the  $i$ th subsystem to the  $j$ th subsystem,  $P_{i,diss}$  denotes the power dissipation of the  $i$ th subsystem,  $\omega$  denotes the central frequency of the frequency band,  $\eta_i$  denotes the damping loss factor of the  $i$ th subsystem,  $\eta_{ij}$  denotes the coupling loss factor between the  $i$ th and the  $j$ th subsystem,  $n_i$  denotes the modal density of the  $i$ th subsystem, and  $E_i$  is the average energy of the  $i$ th subsystem.

Under steady-state conditions,  $P_{in} = P_{out}$ , which leads to

$$P_{1,in} = \omega \eta_1 E_1 + \omega \eta_{12} n_1 \left[ \frac{E_1}{n_1} - \frac{E_2}{n_2} \right] \quad (3.15)$$

$$P_{2,in} = \omega \eta_2 E_2 + \omega \eta_{21} n_2 \left[ \frac{E_2}{n_2} - \frac{E_1}{n_1} \right] \quad (3.16)$$

where  $P_{i,in}$  denotes the power transmitted into the  $i$ th subsystem. For a system with three or more subsystems, the interaction can be formulated in a similar fashion. By solving the energy balance equations, the diffusion of the acoustic energy can be obtained.



6.6.2 Stage two

In the second stage, the acoustic analysis tool ACTRAN is used to calculate the noise propagation and the SPL at the hydrophone locations. The same hydrophone locations as for the sea trial and for the propeller-induced noise prediction (Table 6.3) are used here. The average vibration acceleration levels calculated using Designer NOISE in stage one are used as the excitation input for the analysis in ACTRAN. The general methodology that ACTRAN adopts in simulating acoustic power propagation is introduced in Section 6.1. The difference for modeling machinery-induced noise is that an infinite fluid component was applied outside the finite fluid domain to approximate the pressure field on the interface through a truncated multipole expansion. An infinite domain is defined by the following parameters:

- the material of the infinite domain.
- the radial interpolation order.
- the reference ellipsoidal coordinate system (origin and three principal axes), which supports the truncated multipole expansion approximating the sound field; and
- the optional definition of a uniform flow.

6.6.3 Stage three

In the third stage, the predicted SPL for each hydrophone was converted into the RNL compensating for the transmission loss over distance as described in Eq. (3.1).

6.6.4 Analysis results

For the subject vessel, the *CCGS Terry Fox*, the main engines were considered in the analysis as they are the primary machinery noise sources. The impact of other machinery equipment such as pumps and auxiliary engines is insignificant, and thus was not considered in the analysis. The sea trial measured vibration levels of the main engines at the ship speed of 12 knots were used for the analysis. The excitation input from the main engines is shown in Table 6.2.

**Table 6.2 Noise and Vibration Levels of Main Engines of *CCGS Terry Fox***

	Octave Band Frequency, Hz							
	31.5	63	125	250	500	1000	2000	4000
<b>Airborne Noise @1 m, dB re 20 μ Pa (Measured)</b>	61.3	74.4	83.6	90.7	96.6	98.0	96.9	91.6
<b>Foundation Vibration, dB re 1 μG (Measured)</b>	58.7	58.6	58.7	57.7	54.5	62.5	62.8	58.8

The vibration acceleration levels of the hull were calculated by Designer NOISE, and the results are shown in Table 6.3. Figure 6-18 below shows the cutaway model of the CCGS Terry Fox in Designer Noise.

**Table 6.3 Vibration Acceleration Level of Hull, dB re 1 µg**

Subsystem	Octave Band Frequency, Hz							
	31.5	63	125	250	500	1000	2000	4000
Shell1	0.0	15.0	24.0	29.4	33.0	33.8	30.7	19.1
Shell222	18.8	26.9	36.7	43.8	49.7	53.5	50.9	41.5
Shell226	12.0	21.8	31.3	37.6	42.5	45.0	42.6	32.6
Shell27	25.5	36.0	46.3	54.0	59.6	63.3	62.3	53.5
Shell29	29.8	39.8	50.3	58.1	63.8	67.5	67.1	58.6
Shell34	11.5	22.4	32.2	39.0	43.9	46.8	44.4	34.5
Shell37	18.5	29.0	38.9	46.2	51.5	54.7	52.9	43.5
Shell42	9.3	20.3	29.7	36.2	40.8	43.1	40.2	29.8
Shell46	15.9	26.1	35.9	42.9	48.0	51.1	48.7	39.0
Shell50	21.4	30.7	40.5	47.8	53.5	57.2	54.7	45.4
Shell54	37.4	44.2	54.3	61.9	68.7	73.5	70.9	62.5
Shell133	8.2	19.0	28.2	34.1	38.2	39.7	37.1	26.1
Shell55	34.8	42.2	52.2	59.9	66.7	71.6	68.5	59.9
Shell58	36.6	43.7	53.9	61.6	68.3	73.0	70.5	61.9
Shell68	35.1	42.4	52.8	60.5	66.8	71.3	69.9	61.6
Shell69	28.9	37.5	47.6	55.2	61.2	65.4	63.5	54.8
Shell70	30.7	39.0	49.2	56.7	62.6	66.5	65.4	56.8
Shell77	31.8	42.1	52.9	61.0	66.9	71.1	70.5	62.1
Shell80	30.0	37.8	47.8	55.1	61.3	65.4	62.9	53.8
Shell9	16.1	26.4	36.3	43.0	47.9	50.3	48.8	38.9
Shell14	12.6	23.5	33.0	39.2	43.4	45.2	42.9	32.2
Shell19	26.5	36.7	47.0	54.4	59.7	62.9	62.3	53.3
Shell21	22.9	32.8	42.8	49.8	55.0	57.9	56.6	47.2
Shell214	10.5	19.7	29.3	35.8	40.9	44.0	41.4	31.6
Shell215	18.8	27.9	37.6	44.5	49.8	52.9	50.7	41.1
Shell221	8.7	19.0	28.3	34.2	38.6	40.8	37.9	27.5

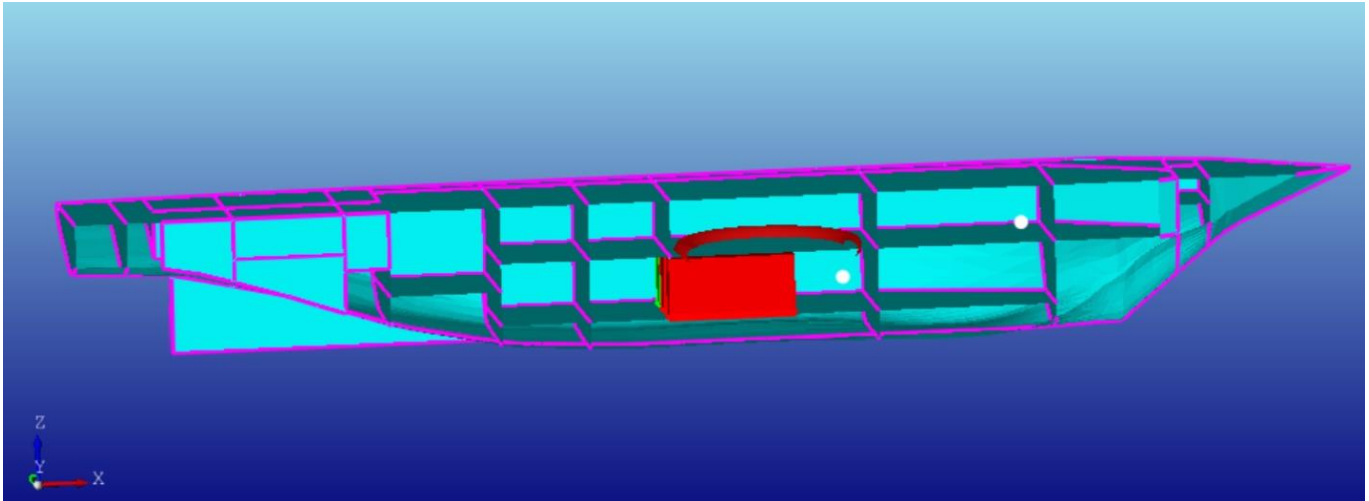


**Figure 6-18 Cutaway view of the structure-borne noise model in Designer NOISE**

The noise model using ACTRAN is shown in Figure 6-19 . Six hydrophones were employed; their coordinates are shown in Table 6.4 below. The calculated SPL at the six hydrophones are shown in Table 6.5. The transmission losses are calculated based on the distance between the hydrophones and the acoustic center of the vessel (taken as the port propeller center). The calculated transmission loss for the six hydrophones is shown in Table 6.4.

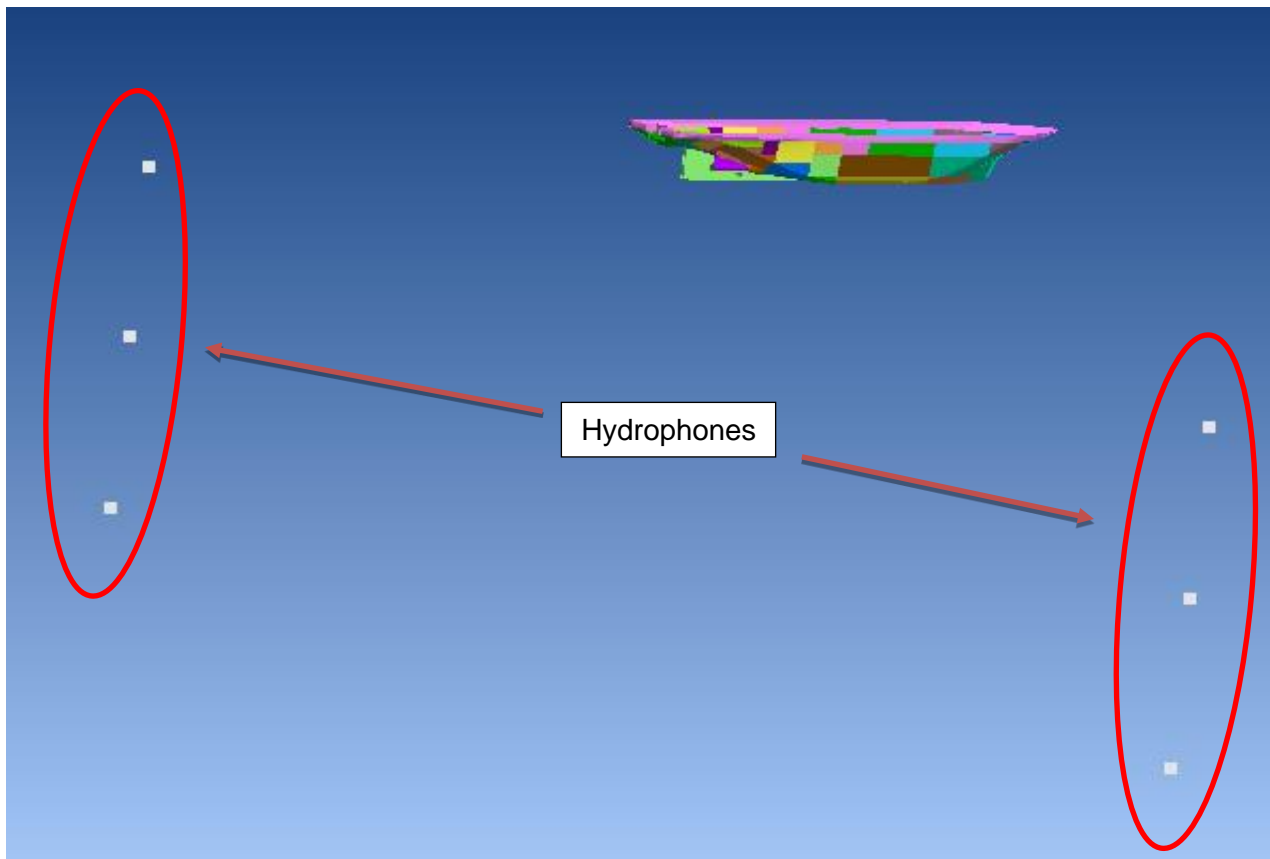


**Figure 6-19 Acoustic model in ACTRAN for predicting impact of the machinery-induced noise**

**Table 6.4 Hydrophone Locations for acoustic analysis of the machinery-induced noise**

No	dCPA, m	Distance aft AP, m	Depth, m
1	154.9 (Port)	2.4	32
2	154.9 (Port)	2.4	64
3	154.9 (Port)	2.4	96
4	154.9 (Starboard)	2.4	32
5	154.9 (Starboard)	2.4	64
6	154.9 (Starboard)	2.4	96

**Table 6.5 Calculated Sound Pressure Levels at Hydrophones**

Sound Pressure Level, dB ref 1 $\mu$ Pa						
Freq/Hz	No.1	No.2	No.3	No.4	No.5	No.6
31.5	109.6	107.4	102.4	109.6	107.4	102.3
40	108.3	106.0	100.8	108.3	106.0	100.8
50	112.5	109.4	103.6	112.5	109.4	103.5
63	110.4	107.1	100.8	110.4	107.0	100.8
80	110.5	107.2	101.6	110.5	107.3	101.6
100	119.9	119.5	116.8	119.8	119.5	116.8
125	118.3	120.2	117.6	118.3	120.2	117.6
160	116.3	117.8	114.4	116.3	117.8	114.4
200	116.3	120.9	121.3	116.3	120.8	121.3
250	108.3	108.7	115.3	108.4	108.7	115.3
315	110.3	117.4	118.1	110.3	117.3	118.0
400	114.3	113.9	121.1	113.7	112.4	121.3
500	112.1	119.7	116.4	110.1	119.5	116.7
630	111.9	119.7	109.2	109.9	118.9	108.3
800	89.0	113.6	106.2	107.2	114.6	103.0
1000	111.7	107.6	112.7	105.7	111.3	115.6
1250	114.6	104.3	112.7	113.5	95.6	115.4
1600	105.9	87.5	111.2	115.0	108.8	115.2
2000	104.2	104.6	107.0	96.5	105.2	110.3
2500	110.5	93.8	103.1	109.6	107.7	112.6
3150	101.6	102.6	97.4	108.1	93.9	99.9
4000	108.1	84.5	102.7	98.1	93.7	101.8

**Table 6.6 Transmission Loss for Six Hydrophones shown in Table**

	No. 1	No. 2	No. 3	No. 4	No. 5	No. 6
TL	45.0	44.3	43.9	45.0	44.3	43.9

The average RNL based on the RNLs calculated from each hydrophone is shown in **Figure 6-20**. Table 6.7 shows the machinery-induced signature source level of the vessel.

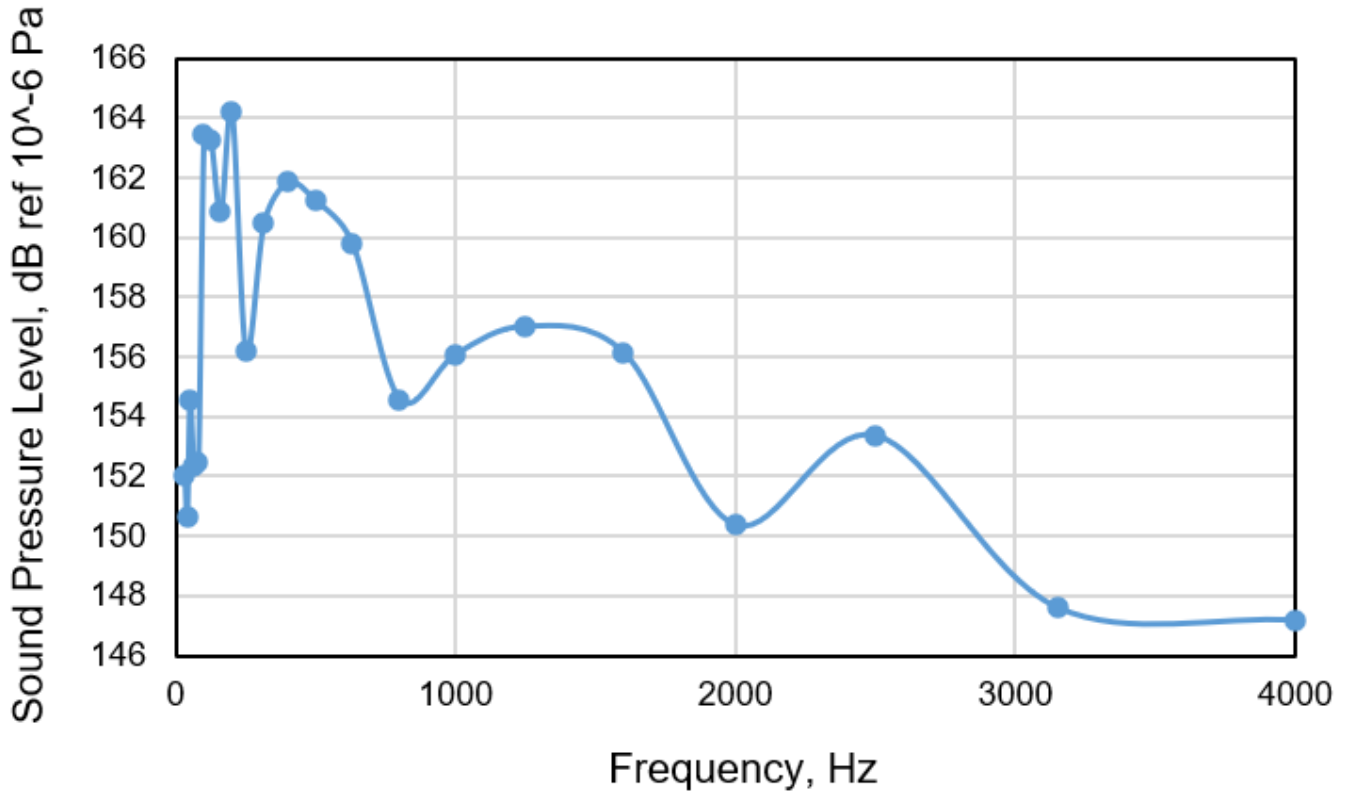


**Figure 6-20 Machinery-induced signature source level of the Terry Fox**

**Table 6.7 Machinery-induced signature source level of the Terry Fox**

Frequency/Hz	Sound Pressure Level, dB ref 1 $\mu$ Pa
31.5	152
40	151
50	155
63	152
80	152
100	163
125	163
160	161
200	164
250	156
315	161
400	162
500	161
630	160
800	155
1000	156
1250	157
1600	156
2000	150
2500	153
3150	148
4000	147

**Figure 6-21** shows the comparisons of combined RNL (structure-borne noise and propeller induced noise) and the measurement data. The combined results are in good agreement with the measurement data, with differences of approximately 5 dB.

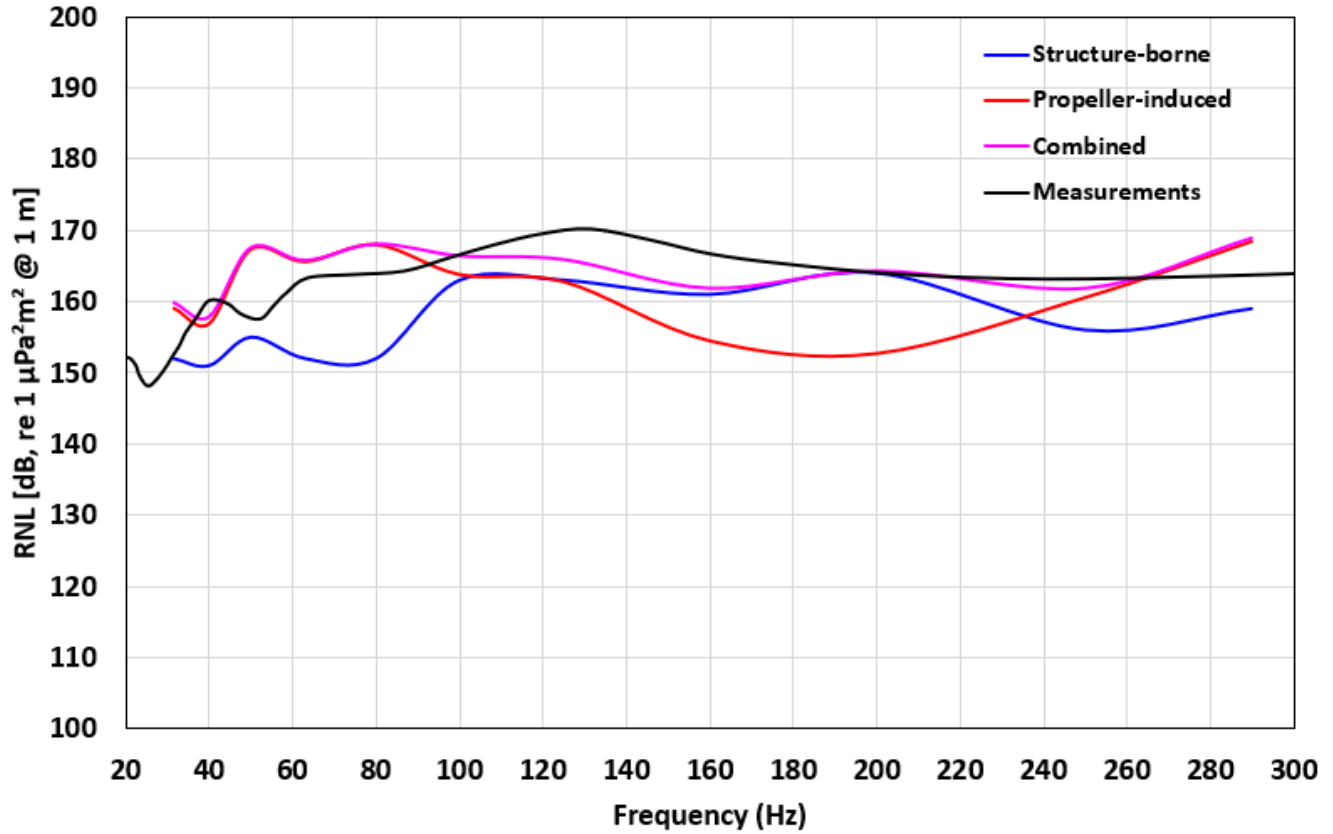


Figure 6-21 Comparisons of the combined RNL (structure-borne noise and propeller-induced noise) and the measurement data

## 7 Discussion

To compare the applicability of different methods for predicting vessel-induced URN, the obtained RNL spectra by different methods are presented together in **Figure 7-1** and **Figure 7-2** for a lower frequency range (20 to 300 Hz) and a much broader range (10 to 10,000 Hz), respectively. The RNL spectrum based on the Ross-Fraser model was selected as representative for the low-fidelity empirical methods. The high-fidelity RNL spectrum includes two components: (1) the propeller-induced noise, which was obtained by averaging the RNL of the three hydrophones as described in Section 6.4.4, and (2) the structure-borne noise as calculated in Section 6.6.4.



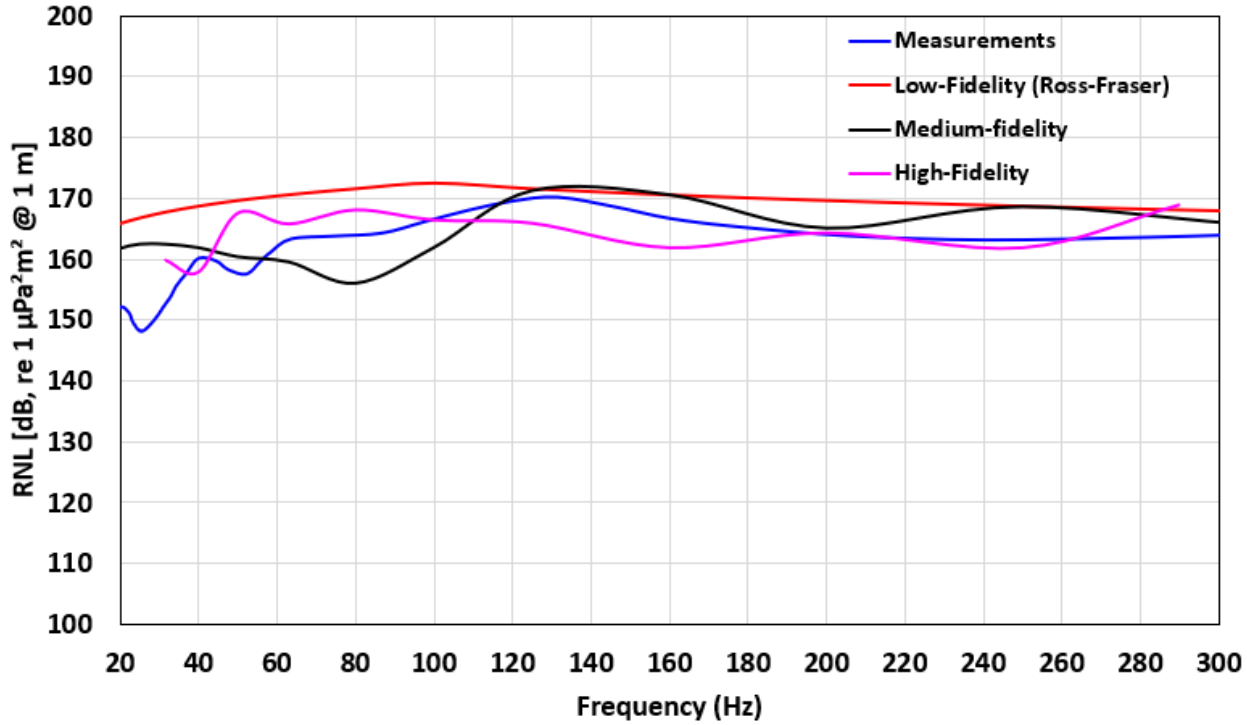


Figure 7-1 Predicted URN levels by different methods and compared to the measurement results from the sea trial for lower frequency range (less than 300 Hz)

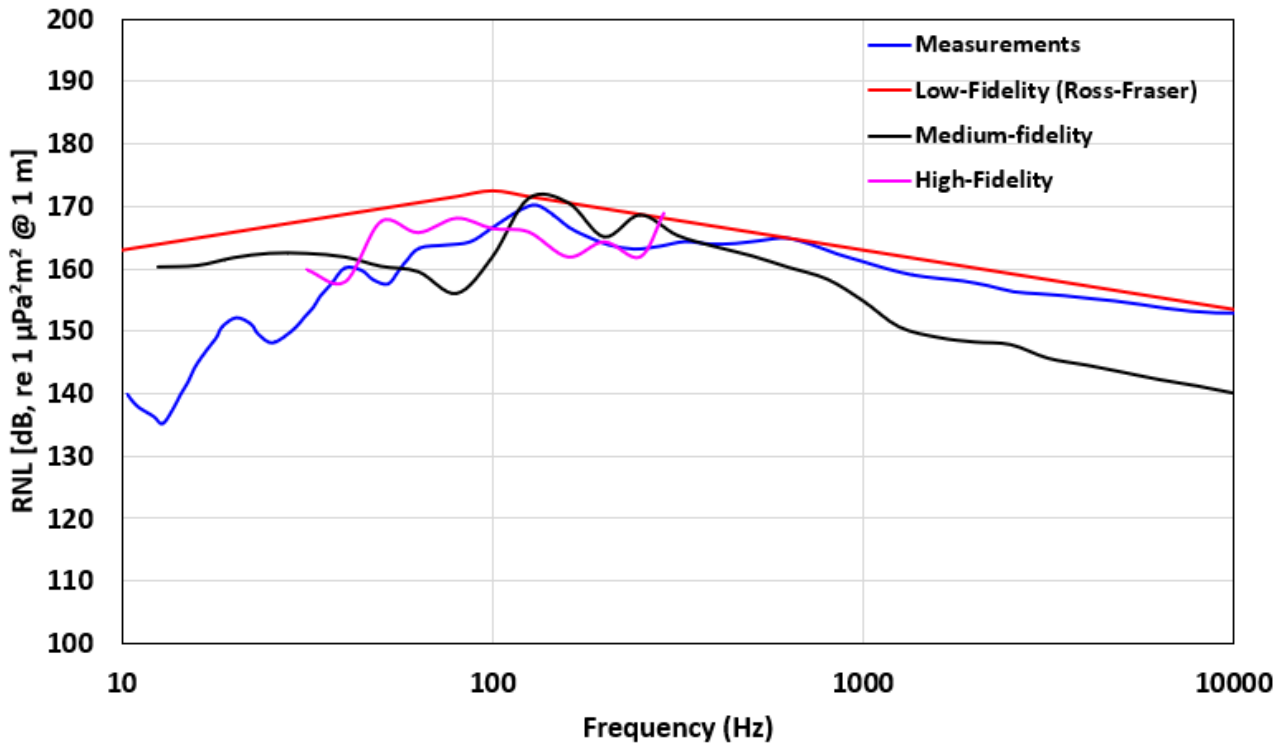


Figure 7-2 Predicted URN levels by different methods and compared to the measurement results from the sea trial for broadband frequency range (10 to 10,000 Hz)

Overall, the predicted noise levels by the different methods are in reasonable agreement with the measurement data. Impressively, the noise levels based on the low-fidelity empirical model provided a plausible upper bound for the noise spectra from other sources, overpredicting the RNL by only 5 dB for the frequencies above 120 Hz. Given the very low resources it requires to implement, the empirical model provides a good starting point for the early design stage.

The medium-fidelity method, i.e., the combined BEM simulation and cavitation models, achieved better agreement with the measurement data for the frequency range below 1,000 Hz. Relatively large discrepancies (up to 15 dB) occurred in the lower frequency range (lower than 40 Hz) and the higher frequency range (above 1,000 Hz). For the high-fidelity method (combining the propeller-induced noise and the structure-borne noise), the predicted noise levels agree reasonably well with the measurement data. However, some discrepancies can still be observed over the frequency range from 20 to 300 Hz. The causes for the discrepancies in the high-fidelity model results compared to the sea trial measurement might include:

- The possible underprediction of the cavitation impact, which would dominate the frequency range between hundreds and tens of thousands of Hz of the CFD simulation.
- The inadequacy of the CFD simulation in detecting significant tip vortex cavitation (**Figure 5-7**). In fact, only minor cavities were detected along the tip of the blade at the top dead center. Although the spiral tip vortex was clearly identified no actual cavitation was found appreciable. This might be due to the inadequacy of the CFD model, in particular, the cavitation solver. As a result, the noise spectrum predicted using the high-fidelity method was missing some contributions for the medium frequency range (between 120 and 250 Hz).
- The CFD simulation was conducted at model scale. The wake flow was only generated by an aftbody of the hull. This treatment was due to the limited computational resources and the best practices for full-scale full-ship cavitating propeller simulation still being in development. Some errors might have been created due to the scaling factors.
- The RANS-based CFD model smeared the fine eddying structures of turbulence around the propeller. The turbulence-induced noise was considered secondary and was omitted in the acoustic model. This treatment was also based on the understanding that no significant tip vortex cavitation was detected from the CFD results.
- The Lighthill surface could have been created to better conform to the blade envelope. Some blade loading could have been lost between the actual blade surfaces and the Lighthill surfaces.

## 8 COMMERCIAL SYSTEM DESIGN AND DEVELOPMENT

The following description outlines the work performed in the design of a commercial version of a shipboard vibration data collection system comprising an accelerometer interface unit capable of simultaneous sampling of up to 8 cabled accelerometers mounted within 10 m of each interface. The work included systems design and product engineering for an installation capable of supporting up to 4 of these accelerometer interface units capable of connecting a total of 32 accelerometers, making the concept suitable for dual engine designs with instrumentation on both engine beds, as well as the internal hull close to the propellers.

### 8.1 Work Completed

The following description outlines the work performed in the design of a commercial version of a shipboard vibration data collection system comprising an accelerometer interface unit capable of simultaneous sampling of up to 8 cabled accelerometers mounted within 10 m of each interface. The work included systems design and product engineering for an installation capable of supporting up to 4 of these accelerometer interface units capable of connecting a total of 32 accelerometers, making the concept suitable for dual engine designs with instrumentation on both engine beds, as well as the internal hull close to the propellers.

### 8.2 Overall Design Approach

The overall electronics design was based around two key concepts: an 8-channel wideband A-to-D converter with simultaneous sampling on all channels, and a Linux processor implementation with built-in Google Machine Learning capability (Google Coral) as the main local processor. To ensure simplicity of integration on the vessel, the accelerometer interface unit is powered by Power-over-Ethernet (PoE), meaning a single Ethernet cable is all that is required for the interface to be fully energized and communicate. The Ethernet connection provides the advantage of full electrical isolation for both data and power and enables connection of multiple units through connection to a standard PoE Ethernet switch. The Ethernet switch output provides a combined data feed from all interface units to the data processing and display system, comprising a standard small form-factor PC with display, located where convenient for crew reference. The 100 m maximum Ethernet segment length, when combined with the required PoE switch to power the system, supports a configuration suitable for most vessels, while remaining extendable as required.

For the sensing elements, piezoelectric shear accelerometers are the de facto standard, and the test program selected the Piezoelectronics Model 352C33 units as small and easily mounted to location by various methods. These methods can include drilling and tapping a mounting hole (not possible on the ship structure), employing a magnetic base (not preferred due to limitation imposed on the frequency response), and alternatively, cleaning the steel plate surface and using cyanoacrylate adhesive to fix the base in location.

Laboratory tests conducted previously by Dr. Lorenzo Moro indicated that the cyanoacrylate mounting method, when done properly, can provide up to 8kHz of response bandwidth. This was considered important to capture cavitation harmonics (less so for the lower frequency engine vibrations) and was selected as preferred method. An accelerometer of the type selected is shown in the photo below (**Figure 8-1**).



**Figure 8-1 PCB Piezotronics Accelerometer**

The accelerometer interface unit comprises an Ethernet-output digitizer with a 32-bit A-to-D resolution and a 44.1 kHz digitization rate. The unit is designed with built-in Integrated Electronic Piezo Electric (IEPE) power supply for direct connection to the selected piezo-electric accelerometers. A single unit can connect 8 accelerometer sensors, each feeding into a hardware adjustable variable gain stage pre-amplifier with 4 selectable gain settings (6dB, 12dB, 20dB and 26dB), followed by a 4th order Butterworth low pass filter with an 8 kHz cutoff frequency.

For improved electrical noise performance, the accelerometer signals are presented to the A-to-D converter as differential signal pairs, and digitized by low-noise, sigma-delta audio converters (ADCs) of the TLV320ADC6140 family by Texas Instruments. Features of this IC include internal filtering that can be applied during digitization by implementing programmable digital processing blocks that include phase calibration, gain calibration, high-pass filtering, digital summing, mixing, bi-quad filter topologies, and volume control.

The brain of the accelerometer interface unit is an onboard Google Coral System-on-Module (SoM), that integrates an embedded Linux system with NXP's iMX8M system-on-chip (SoC), and Google's Edge TPU coprocessor for machine learning (ML) acceleration. This powerful combination has the potential to

perform post-digitization processing through ML before saving the data to the onboard microSD card slot or offloading the data through the main 1000Mbps Ethernet connection. Additional connections to the SoM include a USB type C port with full USB 3.0 capabilities and a micro-USB port for basic Serial to USB communications.

The system Power-over-Ethernet is implemented using Silvertel's Ag9900 PoE module which is IEEE802.3af compliant and outputs a guaranteed 12 Watts at 24VDC. When connected to a 1000Mbps PoE Power Source Equipment-capable switch, power is available to the receiver over the full Ethernet segment distance of 100 m CAT5e cable, supporting system installation in remote areas of the ship where electrical power may otherwise be inaccessible. This capability supports efficient installation with a minimum of issues on many vessel types.

The accelerometer interface unit packaging is in a standard electronics enclosure from Lansing Instrument in the USA. The packaging is suitable for dry, protected locations on board a vessel such as the engine room or other internal machinery spaces, the rudder control room or adjacent area. **Figure 8-2** and **Figure 8-3** show the packaging configuration from frontal and rear views.



**Figure 8-2 Accelerometer Interface Unit with Google Coral Machine Learning capable Linux OS processor**



**Figure 8-3 Accelerometer Interface rear panel showing 8 inputs for PCB Piezotronics 352C33 accelerometers**

Internally, the interface comprises a six-layer printed circuit board designed in-house by E Sonar Inc (**Figure 8-4**). The multi-layer design simplifies routing by using dedicated layers for DC power, ground, low-noise analog signals, and high-speed digital signals. A major benefit is the ability to closely couple a ground layer below a high-speed signal layer or analog signal layer to provide controlled trace impedance for predictable signal propagation, clean rise times, and lower noise generation and susceptibility. When connected to cabling and sensors the assembled unit would look as shown in **Figure 8-5**.



**Figure 8-4 Printed circuit board model showing the placement of key components and PCB outline to fit the selected enclosure**



**Figure 8-5 Assembled unit connected to cabling and sensors**

### **8.3 Path to Completion and Commercialization**

the work has included development of a more commercial instrumentation setup capable of obtaining vibration measurements from multiple locations inside the vessel and aggregating the resulting data to allow subsequent signal processing calculations to support meaningful presentation of the instantaneous noise signature of the vessel to the operational crew in real time. This report outlines the system design approach taken, the data aggregation, distribution, processing, and display, while providing an overall design (with work still to complete) that can provide this capability in a commercial package that can be retrofitted for ship owners.

Completion of the commercial embodiment of the noise measurement system will necessarily comprise a progression of technical and engineering steps. These are outlined below with brief notes on the complexity and effort required.

#### **8.3.1 Review and finalize schematic and PCB layout for initial fabrication.**

The engineering design completed to date was built from an extension of prior IP developed by eSonar Inc. and intended for digitizing piezo-electric hydrophone signals. This approach lowered development risk by limited new design modifications to those necessary to accommodate accelerometer interfacing, Power-over-Ethernet, differing sample rates and resulting data volumes. Multilayer PCB printing, shipping and inspection charges plus engineering design time make up the cost to complete.

Complexity to complete: Moderate; Risk Low, estimated cost for this task \$20,000.

### **8.3.2 Build and test prototype hardware and verify device drivers.**

This work will require electronic part sourcing and purchase, initial PCB population and systematic testing and production of 2 to 3 prototypes to support testing of software and device driver code. Parts specification, acquisition cost, and engineering time to test and confirm functionality make up the cost for this task.

Complexity: High; Risk Moderate; cost for this task \$10,000.

### **8.3.3 Write data handling code for Coral data logging/storage in removeable media.**

This work requires code development on the Coral system, some of which can be completed on a development system implementation currently available for use, and some work will require a functional prototype assembly prepared as an output from the tasks above.

Complexity: Moderate; Risk: Moderate; estimated cost for this task \$20,000.

### **8.3.4 Write Ethernet data transfer software for transmission to computer.**

The data obtained from sampling the accelerometers at a suitable rate must be formatted, uniquely identified, and queued for transmission over Ethernet. Ideally, an existing format for transmitting sampled data can be adopted or extended to meet the requirement. The work will include code preparation for transmit and reception, testing of same and verification with either actual data from prototype hardware or simulated data from the storage media.

Complexity: Low; Risk: Low; estimated cost for this task \$10,000.

### **8.3.5 Build and integrate full system and calibrate accelerometer response.**

With both software and hardware developments advanced to full functionality there will be a need to validate and calibrate the accelerometer response using the full system implementation on a vibration table with comparison to a calibrated standard. This work should validate all 8 channels and demonstrate interchangeability of the channels.

Complexity: Low; Risk: Moderate: estimated cost for this task \$10,000.

### **8.3.6 Prepare signal processing and display software for crew-facing system.**

A remote system, located on the bridge or other suitable area, will receive the sampled Ethernet data stream comprising vibration data from the accelerometers, and run this data through custom designed signal processing algorithms developed for this purpose and based on the research outcomes. The processed data will be displayed in numerical and graphical formats to inform the crew of the current status of the vessel URN signature. It is the intention of eSonar to hire a new PhD from Memorial University to work on this capability, supported by staff electrical and computer engineers.

Complexity: High; Risk: High; estimated cost for this task \$60,000.



**8.3.7 Write API for integration with third party systems.**

It is fully expected that data and algorithm integration into existing ship systems will be a request of customers especially as integrated bridge systems comprise the crew interface on many new vessels. To accommodate this, there is a need to develop an Application Programming Interface that will allow this vibration data to be accessed from the main Ethernet system data feed, processed, and displayed as and where necessary to maximize crew benefit. This will allow integration with third party systems while protecting the project IP for commercial exploitation.

Complexity: Moderate; Risk: Moderate; estimated cost for this task \$40,000.

**8.3.8 Deploy test system onboard a vessel of opportunity selected for best value proposition including opportunity for validation and follow-on marketing.**

The fully functional system will be installed on a selected vessel that will be navigating in an area where URN is a current or pending concern. This could be a large fishing vessel in Nunavut, an offshore supply tug off Newfoundland, or a CCG ship involved in coastal patrol. Ideally, this will be paired with a Class and/or academic research program that can leverage the technology and utilize the data to advance this area of research.

## 9 CONCLUSIONS

To improve the methodologies, models, and tools for predicting ship-induced URN, a dedicated sea trial was conducted. The *CCGS Terry Fox*, a twin-screw icebreaker, was selected as the subject vessel because of the availability of the drawings, 3D scanned data, and numerical models to start with. The sea trial followed the procedures as laid out by the relevant ABS requirements [1] and collected useful data including onboard measurement of the machinery-induced noises and the URN picked up by the hydrophones.

With the sea trial collected, a series of predictive modeling was conducted. To accommodate different needs from the maritime industry, different levels of modeling techniques were adopted:

- Low-fidelity methods, based on empirical models with broad applicability and can be implemented with the minimum resources and effort.
- Medium-fidelity methods, based on numerical simulations of the propeller-induced flow and additional models to address the impact of sheet and tip vortex cavitation, requiring medium amount of resources and effort.
- High-fidelity methods, based on CFD and computational acoustics as well as SEA-based machinery-induced noise power transfer, with high demand for resources and effort.

The predicted noise spectra using low- and medium-fidelity methods showed good agreement with the sea trial measurement results over the frequencies lower than 300 Hz. The predicted noise spectra by the low- and medium fidelity methods also showed good agreement with the measurements over a much broader frequency range (up to 10,000 Hz). The results suggest that these two classes of methods have great potential in predicting ship-induced URN for practical applications.

The high-fidelity method also showed good agreement with the measurement results for frequencies between 20 and 300 Hz. It would also require prohibitive resources for the analysis to reach a frequency higher than 300 Hz. Some possible improvements of the modeling procedure are discussed in the preceding sections. It appears that the deficit in the predicted propeller RNL curve between 100 and 300 Hz was compensated by the inclusion of the structure-borne noise. That implies that the structure-borne noise, originated as the machinery-induced noise also contributed to the URN significantly in this frequency range.

Through this project several the URN predictive methodologies and tools were tested, with valuable lessons learned. The recommendations developed through this project for further improvement will provide good examples for the industry and will offer insight into the future enhancement of analysis tools and development of classification requirements.

The results also suggest that development of a commercial system is both possible and desirable. Deployment of commercially available equipment for the project's sea trials was successful, yielding useful data for minimal cost.



## Validation of Underwater Radiated Noise Modelling via Specific Ship Measurement

The study suggests that developing and building the first in class system should have a cost below \$200,000 CAD, with subsequent systems having lower costs as preliminary engineering activities are completed.

A key next step in ongoing development of URN modeling is to plan for a follow-on study of the CCGS *Terry Fox* post refit. This will be an opportunity to directly compare the URN profile of an older vessel with the same vessel after a complete refit of the propulsion system and refurbishing of the propellers.

## References

- [1] ABS Guide for Classification Notation Underwater Noise and External Airborne Noise, January 2024.
- [2] User's Manual ABS Ship Propeller Noise Prediction Program, Version 0814a. University of Michigan, 2014.
- [3] BMT, "Evaluation of Propeller Noise Spectrum Technique". Report No. SR36863.01. February 2013.
- [4] A. Angelopoulos, P. A. Fitzsimmons, and A. Y. A. Odabasi, "Semi-Empirical Method for Propeller Broad-Band Noise". British Maritime Technology Limited, 1988.
- [5] User's Guide PROCAL, Version 2.4. CRS Report No. 28652-9-RD, September 2018.
- [6] A. E. Raestad, "Tip vortex index – An engineering approach to propeller noise prediction". The Naval Architect, July/August, 1996.
- [7] MARIN, "Development of an empirical model for the hull pressures and radiated noise by a cavitating tip vortex – Part I: Development of the source strength model". Report No. 23687-5-RD. May 2013.
- [8] MARIN, "Development of the ETV-method Version 2: A semi-empirical method for broadband noise from tip vortex cavitation". Report No. 28040-4-RD. May 2017.
- [9] MARIN, "Incorporating tonals and cavitating flow results in the Empirical cavitating Tip Vortex (ETV) model". Report No. 30325-2-RD. March 2020.
- [10] MARIN, "A concise user's guide to the 'Dynamic Bubbles APP'". 28040-3-RD. July 2017.
- [11] M.J. Lighthill, "On sound generated aerodynamically: I. General theory", Proceedings of Royal Society London, Vol. 211, 1952.
- [12] Hexagon AB, "ACTRAN 19.1 User's Guide", 2019.
- [13] V.M. Viitanen, A. Hynninen, T. Sipila and T. Siikonen, "DDES of Wetted and Cavitating Marine Propeller for CHA Underwater Noise Assessment", Journal of Marine Science and Engineering, May 2018.
- [14] OpenFOAM User Guide: Cyclic Arbitrary Mesh Interface (AMI), <https://www.openfoam.com/documentation/guides/v2112/doc/guide-bcs-coupled-cyclic-ami.html>
- [15] J. A. Szantyr, "Scale effects in cavitation experiments with marine propeller models", POLISH MARITIME RESEARCH, No. 4, 2006.
- [16] P. W. Smith and R. H. Lyon, Sound and structural vibration, Office of Technical Services, U.S. Department of Commerce, 1965.

## CONTACT INFORMATION

**Matthw Thomas, P.Eng**

Principal Engineer

ABS Canada Inc

(343) 633-1464

Email: [MatThomas@eagle.org](mailto:MatThomas@eagle.org)

**James Bond, P.Eng**

Director, Polar Research & Ice Class Ships

Director, Business Development

ABS Canada Inc

Direct: (343) 633 1405

Mobile: (832) 312-9489

Email: [JBond@eagle.org](mailto:JBond@eagle.org)

**NORTH AMERICAN REGION**

1701 City Plaza Drive

Spring, TX 77389

United States

**SOUTH AMERICAN REGION**

Rua Sao Bento 29-11 Floor,

Centro Rio de Janiero

20090-010 Brazil

**EUROPE and AFRICA REGION**

ABS House

No.1 Frying Pan Alley

London E1 7HR, UK

**MIDDLE EAST REGION**

Al Joud Center

1st Floor, Suite #111

Sheikh Zayed Road

P.O. Box 24860, Dubai

United Arab Emirates

**GREATER CHINA REGION**

World Trade Tower, 29F

Room 2906

500 Guangdong Road

Huang Pu District

Shanghai, 200000 P.R. China

**NORTH PACIFIC REGION**

11th Floor,

Kyobo Life Insurance Building, 7,

Chungiang-Daero,

Jung-Gu, Busan, 48939,

Republic of Korea

**SOUTH PACIFIC REGION**

438 Alexandra Road,

# 08-00 Alexandra Point,

Singapore 119958

Republic of Singapore

© 2024 American Bureau of Shipping

All rights reserved